TECHNIQUES FOR WIDE-AREA STATE ESTIMATION IN POWER SYSTEMS

Robert Fredric Jeffers

A thesis submitted to the Faculty of the
Virginia Polytechnic Institute and State University
in partial fulfillment of requirements for the degree of

Master of Science
in
Electrical Engineering

APPROVED BY

Dr. Jaime De La Ree, Co-Chairman	Dr. James Thorp, Co-Chairman

Dr. Virgilio Centeno, Member

November 29, 2006
Blacksburg, VA

TECHNIQUES FOR WIDE-AREA STATE ESTIMATION IN POWER SYSTEMS

Robert Jeffers

Committee co-chair: Dr. Jaime De La Ree
Committee co-chair: Dr. James Thorp
Department of Electrical Engineering

(ABSTRACT)

Because of a move from Independent System Operators (ISOs) to Regional Transmission Operators (RTOs), a need for real-time wide-area system monitoring has arisen. The state estimator (SE) is the tool currently used in power systems for real-time monitoring. Because current SE techniques become operationally expensive on such large systems, it is beneficial to consider alternate methods for wide-area state estimation (WASE). In particular, hierarchal methods for WASE become beneficial for large systems because of their speed of operation and relatively low data volume. This study tests four hierarchal WASE methods - two taken from literature, and two developed by the author – and compares them with the use of an integrated wide-area estimator. Additionally, because of their accurate and readily available measurement capability, the inclusion of phasor measurement unit (PMU) data in the WASE methods is examined. For the purpose of realistically integrating an RTO WASE with current ISOs, the methods are constrained so that they do not require sensitive data, nor do they alter the operation of the ISOs SE in any way. The methods are tested for speed of operation, global and local accuracy, and robustness under bad data and data loss.

ACKNOWLEGEMENTS

Foremost, my sincerest thanks go out to my committee chairs, Dr. Jaime De La Ree and Dr. James Thorp. Their advice and guidance has brought me to this completed work, and has most importantly helped me become a better researcher.

To my third committee member, Dr. Virgilio Centeno, your diligence in seeing your students succeed does not go unappreciated.

I bestow additional gratitude upon the professors that have guided certain pieces of my research, namely Dr. Arun Phadke, Dr. Yilu Liu, Dr. Lamine Mili, and Dr. Serkan Gugercin. Their breadth and wealth of knowledge and experience has been an invaluable resource.

I absolutely thank my parents for giving me their support, love, and encouragement. Through years of teaching, they have instilled me with the determination, thirst for knowledge, and most importantly, the respect necessary to succeed.

Finally, I am extremely grateful for the emotional support selflessly given by all of my friends during my time here. There are quite probably too many to list that have contributed in ways large and small to this completed work.

TABLE OF CONTENTS

LIST OF FIGURES

LIST OF TABLES

Chapter 1 - Introduction

1.1 – Project Motivation

As power system operators undergo restructuring due to deregulation, the functions of power transmission, generation, distribution, and reliability assurance are moving from being performed by vertically integrated companies to horizontally integrated, specialized entities. In the United States between 1996 and 1999, the Federal Energy Regulatory Commission (FERC) allowed for the creation of several Independent System Operators (ISO's) to assume the role of reliability assurance for sections of the power system. In December of 1999, order no. 2000 was issued by FERC which requires any owner of a transmission system to join a Regional Transmission Organization (RTO) [1]. These RTO's were created to increase operation efficiency and reliability on wider scales than ISO's could handle. Among the four descript duties of an RTO is the ability to quickly detect and respond to contingencies, and to direct transmission and generation in the case of an emergency. This duty requires the RTO to have the capacity to monitor its region of the power system in real-time.

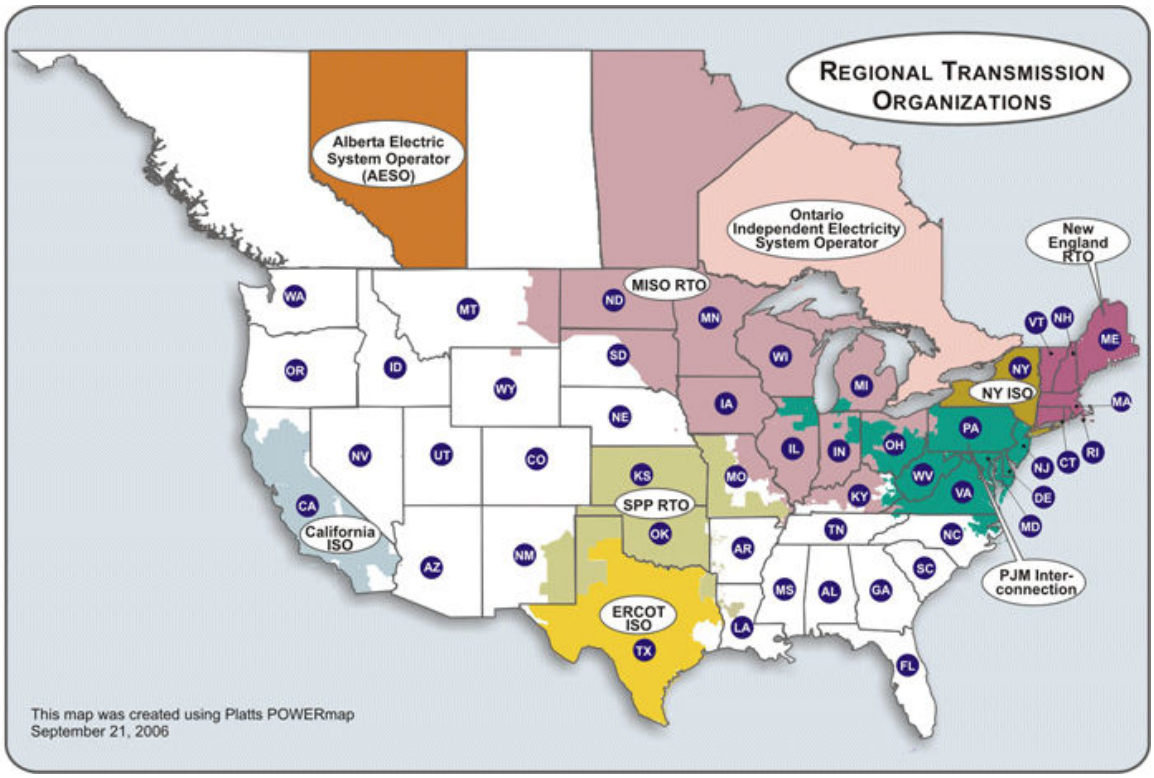

Figure 1.1: RTO's in the United States [23]

As may be viewed in figure 1.1, the power system of the United States is not completely covered by ISO/RTO oversight. Many of the electric utility companies in these uncovered areas are still relatively vertically integrated, meaning that the roles of generation, transmission, distribution, and reliability coordination for an area may fall under the responsibility of a single utility. Individual RTO sponsors, however, have a mediation plan in effect for the creation of a Southeastern RTO. In a submission to FERC, one particular plan states that, upon completion the "properly formed RTO should include all transmission owners in (the southeast) region, including municipals, cooperatives, Federal Power Marketing Agencies (PMAs), Tennessee Valley Authority and other state and local entities" [2]. The plan implicitly mentions that the RTO "will be responsible for directing the operations of the transmission system, monitoring and controlling real and reactive power flows and voltages levels, and scheduling and directing the operation of reactive resources" [2]. Essentially, FERC has determined that reliability assurance can no longer be handled on a small scale, yet system operators are reluctant to provide system information and to give up control.

The task of monitoring wide areas of the power system has been deemed of high importance by FERC for a number of reasons. The first and main motivation is the role wide-area monitoring and control can have on system security and reliability. This manifested itself most recently in the northeastern blackout of August 14 2003. In their final report [3], the U.S.-Canada Power System Outage Task Force showed that even though RTO's are increasing in size, they are insufficient in monitoring complex problems that may manifest themselves, especially near the boundaries of the monitoring area. In figure 1.2 below, key preventable events ensued within the boxed area prior to the major blackout. Due to the fact that problems were manifesting in separate operator's jurisdictions, lack of data sharing between system operators caused problems visualizing the initial causes of the blackout. One of the task force's many recommendations was increasing the role and power of regional reliability councils – operating within the North American Electric Reliability Council (NERC) - to develop the ability among operators to share information in real time such that a complete and accurate visualization of the power system is realizable [3].

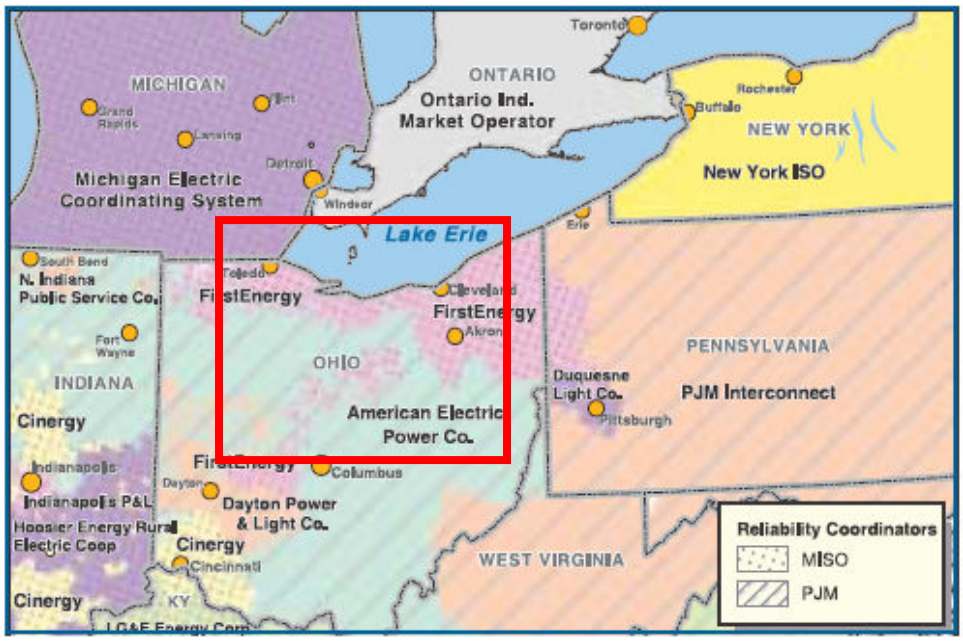

Figure 1.2: 2003 Blackout Operators [3]

Wide area monitoring and visualization brings benefits in addition to security and reliability coordination. In today's deregulated system, power is often bought and sold with little regard to boundaries. For the scheduling of such long-distance power transactions, it is extremely beneficial to have a snapshot of the entire area affected. In addition, because of market regulations and unexpected transactions, parallel flows are beginning to increase in areas between buyers and sellers of power [4]. Because most of these flows are due to outside utility transactions, system controllers are often helpless to take action against such undesirable occurrences. A central reliability coordinator with the ability to monitor the system on a larger scale and the power to direct flows appropriately would ensure the equity of long-distance power transactions. Finally, when undesirable events do occur within the system, it is extremely helpful to have a wide-area snapshot of the state of the system prior to and during the event. Indeed, the timely availability of such visualization may give operators the information needed to prevent another blackout of 2003's proportions.

The essential tool used by system operators for real time analysis of the power system is the State Estimator (SE). The SE acts to filter errors in the system measurements by

computing the optimal bus-bar voltage state based on the redundant raw information available. This voltage estimate is used to monitor and analyze the current static state of the system. Because of the SE's inherent data concentration, it has been proposed [4-9] that information sharing for visualization be placed post-SE processing, as illustrated in figure 1.3. This study proposes that such a wide-area state estimate (WASE) be used as the tool used for wide area monitoring and visualization of the power system.

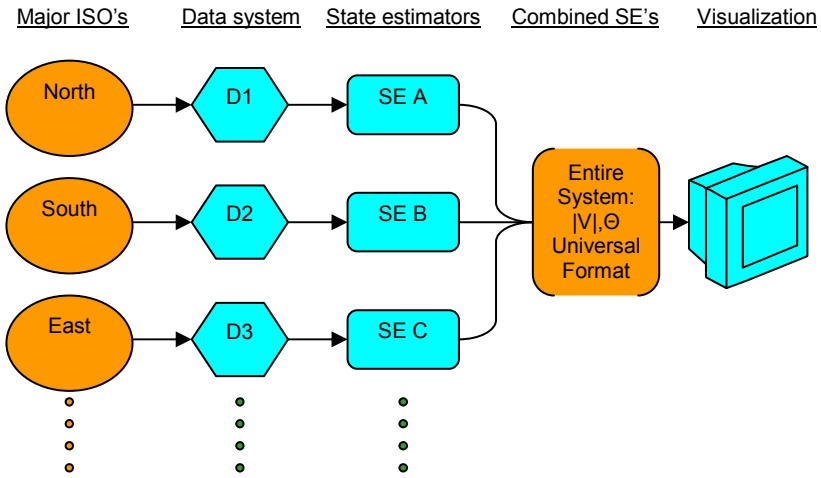

Figure 1.3: Post-processing Wide Area Visualization

The phasor measurement unit (PMU) is a power system device capable of measuring the synchronized voltage and current phasor in a power system. PMUs are quickly becoming the ultimate tool for wide-area accurate data acquisition [10-12]. Many power utilities have already placed several PMU's in their systems, but currently these PMUs are used mainly for manual data acquisition and post-processing [13]. Because they provide an accurate measurement, PMUs may be integrated into the basic SE for improved local performance. In addition, because PMUs can provide such accurate, synchronized data over wide areas, they are perfectly suited for integration into wide-area monitoring methods, particularly WASE.

1.2 - Thesis Objectives

The main objective of this thesis is to demonstrate the viability of proposed wide-area state estimation methods, and to improve upon such methods using the availability of PMU data. Each method will be scrutinized under three main criteria developed in conjunction with input from system operators and energy suppliers, namely:

1. The operation is as fast as possible so that analysis can be done close to real-time.
2. The method gives an optimally accurate solution for the state of the power system with given measurements.
3. The method is robust enough to contend with the presence of bad data and abnormal operating states.

In addition to these criteria, two constraints are placed upon the WASE methods, namely:

1. To prevent misuse of information, the WASE method will enable monitoring of the entire power system at once while keeping sensitive data private.
2. Cost of implementation to the system operators is minimized by avoiding an alteration in their state estimator function.

Upon rigorous investigation of WASE methods under the proposed criteria, collaboration with system operators will provide the opportunity for tests on actual multi-area power system data. Inasmuch, the completion of work will contribute a test-hardened, implementation-ready method for combining system operator data for real-time monitoring of the power system.

1.3 - Thesis Outline

The thesis is organized into six chapters as follows:

Chapter 1 provides the motivations for WASE and outlines the contributions of this thesis.

Chapter 2 develops the state estimation theory, providing a technical backdrop with which to scrutinize the WASE methods. Newton's method is applied to solve the over-determined set of non-linear power system equations. Run-time of the SE algorithm under large, poorly conditioned systems in examined, along with measures of accuracy and robustness for an SE solution. Measurement error and how it affects the SE are explained, and the concept of bad-data detection is introduced. Two methods of integrating PMUs into the SE are also investigated.

Chapter 3 investigates the current state of wide-area power system visualization, while providing a background of the previous work done towards hardening the WASE method. The chapter also contrasts current methods of WASE in terms of the criteria outlined in section 1.2. The concept of developing an integrated state estimate (ISE) is introduced as a baseline case, in which all power system measurements are shared with the wide-area controller for use in a multi-area SE function. In contrast, the proposed WASE methods fit into a split state estimate (SSE) model, in which the output of the local state estimators are shared to the central controller, who proceeds to combine the solutions in real-time for a complete snapshot of the entire system.

Chapter 4 introduces the algorithms to test the WASE methods in question. In contrast to the baseline ISE method are three SSE combination algorithms. Once data from the area control centers is acquired, the central task for the SSE is to resolve the difference in voltage angle references between the systems. The three algorithms in question differ in their techniques of finding this reference angle difference. Throughout the analysis, no further preference is given to a peer-peer vs. peer-overseer setup. It is assumed that in a peer-peer setup, each peer acts as an overseer to his neighbors, eliminating the need for distinction. The technique to include PMUs into the SSE algorithms is explained, and inference is made into their role in improving the accuracy and robustness of the overall estimate. For purpose of algorithm verification, the individual area SE (IASE) solutions are assumed to be time synchronized.

Chapter 5 demonstrates the results of testing the algorithms and methods introduced in chapter 4. The criteria mentioned in section 1.2 are used to evaluate the SSE algorithms, while the benefit of using PMU data is determined.

Chapter 6 summarizes the key findings of the research, offers areas of future investigation, and comments on the state of wide area monitoring in power systems.

Chapter 2 – Weighted Least Squares State Estimation

2.1 State Estimation in Power Systems

As previously noted, the main goal of the power systems state estimator is to find a robust estimate for the unknown complex voltage at every bus in the modeled network. Since inexact measurements – such as those from a SCADA system - are used to calculate the complex voltages, the estimate will also be inexact. This introduces the problem of how to devise a "best" estimate for the voltages given the available measurements. Of the many criteria used to develop a robust state estimator, the following three are regarded as the most common [14]:

1. Maximum Likelihood: maximizes the probability that the estimated state variable is near the true value.

2. Weighted Least-Squares (WLS): minimizes the sum of the squared weighted residuals between the estimated and actual measurements.

3. Minimum Variance: minimizes the expected value of the sum of the squared residuals between components of the estimated state variable and the true state variable.

In order to study the WASE methods in further depth, it is beneficial to discuss the mathematical basis for the traditional state estimation solution. In this chapter, the WLS method of state estimation is examined in section 2.2, along with its application in power systems. Furthermore, to prove the benefits of a hierarchical method for SE, it is important to examine the nature of the speed of WLS for different sized systems. Inasmuch, the major processor requirements of the WLS method are discussed in section 2.3. Because one of the primary functions of the SE is to perform bad data detection, this methodology is investigated in section 2.4. Finally, section 2.5 introduces measures of accuracy and robustness with which to compare and contrast the proposed WASE methods.

2.2 Weighted Least Squares Method

This study uses the method of weighted least-squares (WLS) state estimation as defined in [14-15] because it has gained popularity among commercial state estimators. Notably, if measurement errors are modeled as having a normal distribution, the WLS method is equivalent to the maximum likelihood method. To begin formulation of the WLS method, the case where the state functions are linear will be considered first, and non-linearity will be addressed subsequently.

First, consider the set of inputs, which are measurements taken from the SCADA system, and express them as functions of the exact state of the system, with corresponding measurement error mainly due to voltage and current transformers:

$$z^{meas} = \begin{bmatrix} z_1 \\ \vdots \\ z_m \end{bmatrix} = \begin{bmatrix} f_1(x) \\ \vdots \\ f_m(x) \end{bmatrix} + \begin{bmatrix} e_1 \\ \vdots \\ e_m \end{bmatrix} = f(x) + e \tag{2.1}$$

where:

f_i = function of the state vector used to calculate the value of the i^{th} measurement

x = system state vector (unknown)

e_i = the error of the i^{th} measurement

For simplicity, the error vector e is assumed to be standard Gaussian, with zero mean and independent covariance. In succeeding chapters, more will be said about these assumptions. Hence:

$$Cov(e) = E(e \cdot e^T) = R = \begin{bmatrix} \sigma_1^2 & & & \\ & \sigma_2^2 & & \\ & & \ddots & \\ & & & \sigma_{Nm}^2 \end{bmatrix}. \tag{2.2}$$

Because of these assumptions, the WLS formulation can be expressed with the following minimization function, which is the sum of the squared normalized residuals:

$$\min_x J(x) = \sum_{i=1}^{N_m} \frac{\left[z_i^{meas} - f_i(x) \right]^2}{\sigma_i^2} \tag{2.3}$$

where:

σ_i^2 = variance for the i^{th} measurement

J(x) = measurement residual function

N_m = total number of independent measurements

z_i^{meas} = quantity of i^{th} measurement

To formulate a vector state equation, the state functions are placed into a vector format:

$$f(x) = \begin{bmatrix} f_1(x) \\ f_2(x) \\ \vdots \\ f_{Nm}(x) \end{bmatrix} \tag{2.4}$$

where:

f(x) = an N_m by N_s matrix containing the coefficients of $f_i(x)$

N_s = number of states in the system

By the same token, the measurements are also placed in a vector:

$$z^{meas} = \begin{bmatrix} z_1^{meas} \\ z_2^{meas} \\ \vdots \\ z_{Nm}^{meas} \end{bmatrix} \tag{2.5}$$

Using (2.1) and (2.3), and assuming an overdetermined system in which there are more measurements than states ($N_m > N_s$) we may write equation (2.3) in a compact matrix form:

$$\min_x J(x) = [z^{meas} - f(x)]^T [R^{-1}][z^{meas} - f(x)] \quad (2.6)$$

To minimize (2.6), the gradient of *J(x)* is equated to zero and simplified:

$$\nabla J(x) = -2[H]^T [R^{-1}] z^{meas} + 2[H]^T [R^{-1}][H]x = 0 \quad (2.7)$$

where:

H = the N_m by N_s Jacobian matrix of f(x)

Solving for x in the equation, and taking into account non-linear f(x), gives:

$$\Delta x^{est} = \left([H]^T [R^{-1}][H]\right)^{-1} [H]^T [R^{-1}](z^{meas} - f(x^{(k)}) = G^{-1} F(x^{(k)}) \quad (2.8)$$

Notice that the notation in equation (2.8) has substituted Δx for x. In the AC power system, voltages are solved in polar coordinates and therefore are not linearly related to measurements such as real or reactive power flow. Therefore, Newton's method is employed to iteratively equate the gradient of J(x) to zero.

2.3 Processor Requirements

In equation (2.8), *G* is called the gain matrix. If the system is fully observable with the given set of measurements, *G* is symmetric and positive definite. Typically, implementation of WLS SE does not invert *G* as shown in (2.8), but instead solves the function using a triangular factorization technique such as Cholesky decomposition. In each iteration *k*, the main processor requirements of a standard WLS SE are [15]:

1. Calculation of $F(x^{(k)})$: flops
   - a. Calculate the measurement function $f(x^{(k)})$ = N_m
   - b. Build the (sparse) Jacobian matrix $H(x^{(k)})$ = $N_m * N_s$
2. Calculation of $G(x^{(k)})$ and equation update step:
   - a. Calculate G from H, R (sparse): = N_m

b. Decompose G into Cholesky factors $= N_s^3/3$

c. Perform forward/back-substitution for $\Delta x^{(k+1)}$ $= 2*N_s^2$

Total calculation expense $= N_s^3/3 + N_m*N_s + O(N_s^2)$ flops (2.9)

Often, it is assumed for purposes of study that the number of measurements N_m is approximately six times the number of states, N_s. Therefore, the total calculation expense can be approximated as:

Total calculation expense $= N_s^3/3 + 8*N_s^2 + O(N_s)$ flops (2.10)

In practice, N_s is large enough such that the N_s^3 term dominates, and therefore a doubling in system size will require roughly eight times the number of flops – or floating point operations - per iteration. Also of note; generally the total number of iterations, k, needed for convergence of Newton's method will increase as system size increases.

2.4 Detection and Elimination of Bad Data

In addition to filtering small random measurement errors, the SE may also provide the function of detecting, identifying, and eliminating gross measurement errors throughout the system. Such large errors tend to occur when meters have biases, drifts, or are simply incorrectly configured [14-15]. Because of its importance in determining the robustness of a WASE, the theory behind bad data detection and identification is explained in this section.

It is first beneficial to broadly categorize the ways in which bad data may appear, namely the case where there is a single bad datum with large error, versus the case where multiple bad data appear. The case of multiple bad data can further be classified into three groups: non-interacting, interacting but non-conforming, and interacting as well as conforming. Non-interacting bad data have weakly correlated residuals, and are therefore are not significantly affected by each other's residuals. In the case of interacting multiple bad data, good measurements can appear to be in error if they are strongly correlated with

bad data. In addition, conforming errors appear consistent with each other, and therefore it is difficult to identify the measurement in error.

The first step in any bad-data filtering algorithm is to detect the presence of bad data. This is commonly accomplished using the Chi squares test. Recall the minimization function (2.3), which minimizes the sum of the squared residuals, J(x), over the system state, x. J(x), being of the form:

$$Y = \sum_{k=1}^{N} X_k^{\,2} \tag{2.11}$$

corresponds to a Chi-square - $\chi^2(N)$ - distribution with N degrees of freedom, assuming X_k follows a standard normal distribution N(0,1). In the case of the objective function *J(x)*, *N* equals (N_m-N_s), which is the number of degrees of freedom (DOF) in the system. This is because, with $N_m > N_s$ in the power system, at most (N_m-N_s) of the measurement errors will be linearly independent. A plot of the $\chi^2(N)$ probability density function (p.d.f.), shown in figure 2.1, represents the probability of finding *J(x)* in the corresponding region. The mean value of $\chi^2(N)$ is DOF=N_m-N_s with standard deviation of $\sqrt{2DOF}$. In the Chi-squares testing method, if the value of *J(x)* is above a set threshold, we say there is a presence of bad data in the SE. The threshold x_t, designated as the dashed line in figure 2.1, is often chosen to constitute a 5% probability of error, or false alarms. For reference in choosing a threshold, tables exist in statistical literature giving Chi-square distribution function values for different degrees of freedom [15].

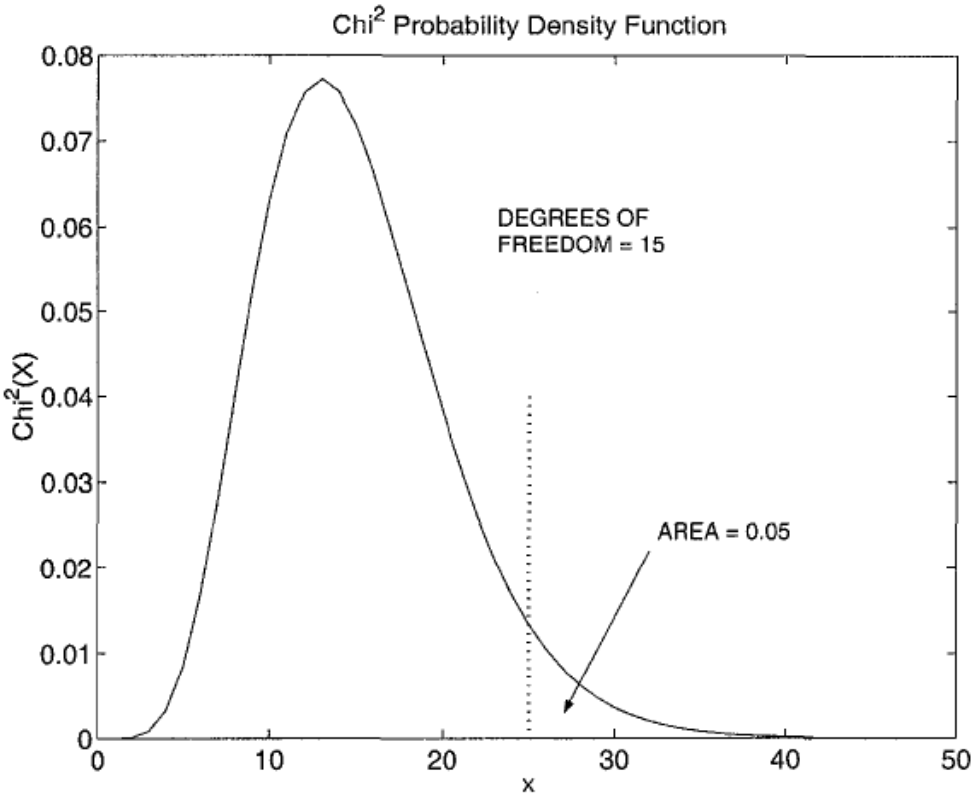

Figure 2.1: Chi Square Distribution

Once detection of bad data has occurred, the next step is to identify the bad data in question. The most common method in power systems SE is the use of the largest normalized residual, or r^N_{max} test. The first step to this method is to calculate the residual for each measurement from the output of the SE, designated as:

$$r_i = z_i - f_i(x) \qquad i = 1,...., N_m \tag{2.12}$$

To normalize the residual, an analysis into the covariance matrix for r is performed. Recall, the update step for x in the WLS state estimator in (2.8). Solving for the estimated value of Δz:

$$\Delta\hat{z} = H\Delta x = HG^{-1}H^T R^{-1}\Delta z = K\Delta z \tag{2.13}$$

K is called the hat matrix, for putting a hat on Δz. Referring to (2.11), and applying some of the properties of the K matrix, the residual can now be defined as:

$$r = \Delta z - \Delta \hat{z} = (I - K)e = Se \tag{2.14}$$

S is called the residual sensitivity matrix, because it describes the sensitivity of the residuals to the measurement errors. Finally, to normalize the residual, the residual covariance matrix is defined using (2.13) and properties of S:

$$Cov(r) = \Omega = E[rr^T] = S \cdot E[ee^T] \cdot S^T = SRS^T = SR \tag{2.15}$$

After the residual sensitivity matrix is calculated, each residual can be normalized:

$$r_i^N = \frac{|r_i|}{\sqrt{\Omega_{ii}}} \qquad i = 1,...., N_m \tag{2.16}$$

Among the normalized residuals, the largest will be designated as bad data if $r_k^N \geq c$, where c is an identification threshold, often 3.0. If bad data is identified, the corresponding measurement is removed and the SE is run again without the bad data.

The Chi-squares test for detection and largest normalized residual test for identification of bad data offers consistently reliable performance under the presence of single bad data, non-interacting multiple bad data, and often under interacting but non-conforming multiple bad data. However, it normally fails to identify multiple interacting conforming bad data. It is the task of the SE operator to examine the residual sensitivity matrix, S. If S_{ik} is large, residuals i and k are highly coupled, and the measurements are therefore interacting. In addition, after experimentation if $r_i^N \cong r_k^N$ on a consistent basis for an error on either measurement i or k, the residuals may be conforming. There are, in literature, SE algorithms that are more robust against bad data, yet their study is not relevant to the comparison of WASE methods.

2.5 Accuracy and Robustness

For WASE, there are several factors that affect the accuracy and robustness of the final estimate. However, to properly judge WASE algorithms against the ISE base case, it is important to have clear-cut measures of accuracy and robustness. Citing the literature [14-16] the common overall indicator of the accuracy of a SE is the value of the objective function J(x). Defined in (2.3), the objective function would be equal to zero if there were no errors on the measurements. When measurements contain errors, however, *J(x)* can be expected to equal the system's degrees of freedom as described in section 2.4. A smaller value for the objective function therefore generally conveys a more accurate estimate of the system state. It is important to mention, however, that *J(x)* is an accuracy rating for the entire estimate. When critiquing the accuracy of one estimated value, for example, it offers no inference. The normalized residuals for the measurements associated with the value in question offer a guide as to the accuracy of an individual estimate [16]. In addition, if one knows the exact state, the error on the estimated voltage magnitudes and angles can be calculated directly. Realistically, the exact state is hardly ever known, but for purposes of algorithm testing the exact state is often a starting point.

In terms an SE's robustness, often the appropriate measure is the sensitivity of the estimator to the quantity and magnitude of bad data present [14]. If the SE converges to an appropriate solution for large errors on limited numbers of measurements, it will be considered statistically robust. Without altering the WLS algorithm, however, there is very little than can be done to consistently detect highly-interacting bad data, as described in section 2.4. Therefore, it is important that the tested WASE implementations be no more sensitive to the presence of bad data than the base case ISE using WLS state estimation.

Chapter 3 – Study on Wide Area Monitoring

In this chapter, the use of PMUs for wide area monitoring is outlined and previous concepts of a hierarchical SE process for WASE are described. Of particular interest is the method known as Split State Estimation (SSE), in which the state variables of separate SE's covering adjunct areas are combined using a fast optimal algorithm with a very small number of accurate measurements [10]. As will be shown, SSE succeeds at significantly decreasing the data volume and processing requirements for the central estimation center.

3.1 Phasor Measurement Units

Phasor measurement units (PMUs) are able to synchronously measure voltage and current phasors within the power system. Using the signal from the satellite-based GPS system as shown in figure 3.1, PMUs are synchronized to within 0.2 μs and available with a reliability of 99.87% [17].

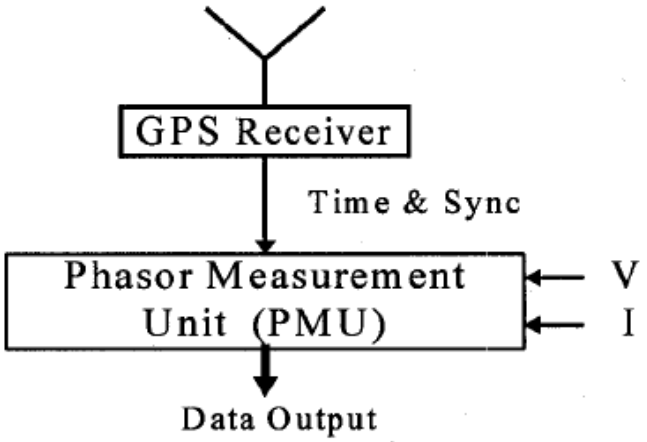

Figure 3.1: PMU Block Diagram

They are able to provide phasor measurements at a rate of up to once per cycle in the form $Ve^{j(\omega t_0+\varphi)}$ with a 0.022 degree error on a 60 Hz system. These abilities make PMUs an important new facet of power system monitoring. Especially intriguing are the applications of PMUs toward wide-area monitoring. Indeed, with proper placement as outlined by algorithms in [18], PMUs introduce the possibility of a real time linear SE. However, providing such a large number of PMUs is a huge economic undertaking.

Therefore, the purpose of this study is to make use of available PMU measurements using the operator's current SE.

3.2 WASE Structure

3.2.1 The ISE baseline

With the continuously growing stature of RTO's, WASE becomes increasingly attractive, if not necessary to supervise large segments of the power system. The traditional method to create a WASE, coined as Integrated State Estimation (ISE) in [8], would pool all SCADA measurements from numerous data concentrators at a centrally located, newly configured control center. This business as usual approach has the benefits of predictability and having industry-accepted tools and algorithms with which to implement it. However, as will be proven, the ISE's drawback lies in its sheer size – the act of polling over a wide area and subsequently running a state estimator with such a large number of measurements and states requires considerable time and computing power.

3.2.2 Hierarchy Benefits

The alternative to ISE – and the emphasis of this study – lies in a hierarchical SE method. The concept of a hierarchical or distributed SE has been proposed in [4-9], and involves distributing the task of data pooling and SE execution among independent coordinated entities. When applied to sharing multiple ISO/RTO SE outputs, the hierarchical SE concept is referred to as a Split State Estimation (SSE) in [10]. As illustrated in figure 3.2, the independent coordinator completes the SSE by using boundary measurements and PMU data to combine the individual operators' SE results. The proposed hierarchical methods share a common benefit, namely, an increase in scope and speed over traditional ISE when applied to multi-area systems. As described further in section 3.3, the two main time constraints on the SE process are that of data pooling and processor time. Data pooling time is defined as the time required to scan the entire SCADA system for measurement updates, and can vary between thirty seconds and five minutes [8]. Once measurements are acquired, the processor time required to run the SE

algorithm constitutes the next major time incurrence. As will be shown, SSE succeeds at significantly decreasing the data volume and processing requirements for the central control center. In total, three criteria and two constraints have been deemed important by those wishing to implement an SSE. Recall that the task of this thesis study, as outlined in section 1.2, is to test SSE decompositions and algorithms on a realistic model, and furthermore to critique the methods based on the aforementioned criteria.

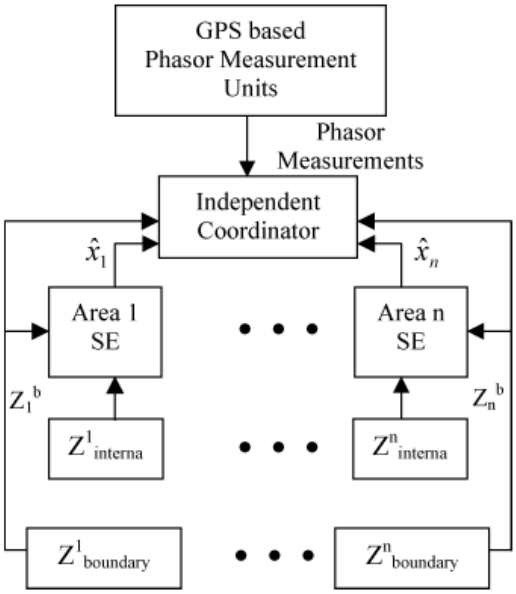

Figure 3.2: Hierarchical SSE Diagram [9]

3.2.3 Method Characteristics

Hierarchical methods for WASE differ based on assumptions such as system decomposition, optimality conditions, information exchange, and bad data detection. To satisfy the criteria outlined in section 1.2, facets of the differing methods are used in this study. Some of the SSE methods of interest are mentioned here:

In the method of the authors in [9], areas are separated by tie-lines, and each area estimates exactly one bus of overlap outside of its region. This boundary decomposition is referred to as common boundary bus ownership, and is described in figure 3.3. Three bus designations exist, namely:

- Internal – all neighboring buses belong to local area
- Boundary – located within local area, but has at least one neighbor from another area

- External – located outside of local area, but has neighbors from local area. Notably, all external buses are boundary buses of an adjacent area.

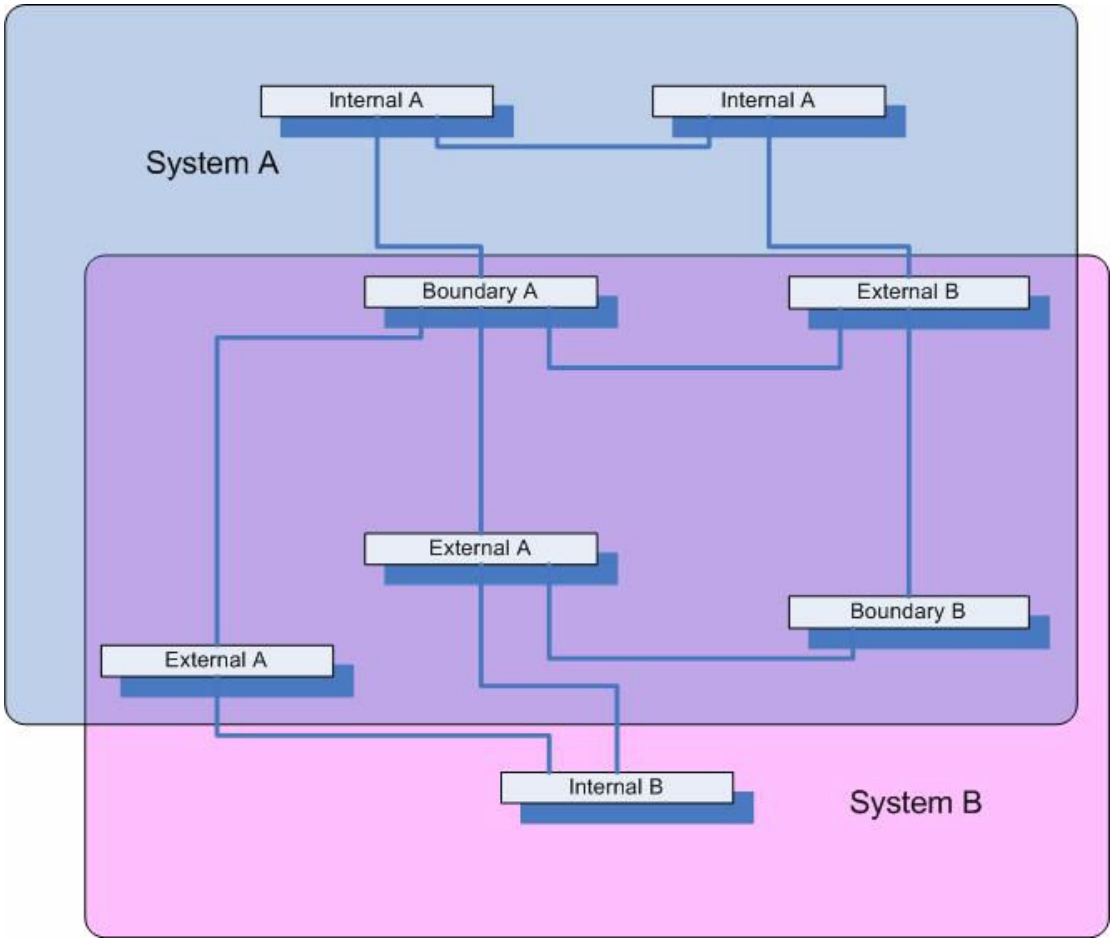

Figure 3.3: Common Boundary Bus Ownership

The task of each area estimator is to eliminate its own bad data and to provide, by any available means, its local state estimate, as well as an updated boundary topology. Additionally, each area must send to the central estimator its state covariance matrix, since the central estimator treats boundary and external bus voltage estimates as pseudo-measurements. This constitutes a large amount of extra data sharing for each SE run. The central estimator's task is to re-estimate the boundary states, and calculate each area's reference angle difference, namely $x_c^{est} = [x_b, \phi_{diff}]^T$. The central algorithm makes use of PMU data to provide redundancy and to check for bad data along the boundary. The solution is locally optimal, but not as accurate as the ISE case.

The method of the authors in [10] separates areas based on bus ownership, and share tie-line measurements between them. Known as common tie-line ownership, this decomposition scheme, shown in figure 3.4, assumes no overlap in the area estimates. Areas often have good equivalent models of outside systems, so it is assumed that their own boundary estimates are acceptably accurate. Individual area SE's are unaltered by the coordination algorithm and the only task of the central SE is to estimate the difference between the areas' reference angles, known as φ_{diff}. The solution is non-optimal and does not include PMU data. However, this method constitutes a minimum of shared data and a fast linear central estimator.

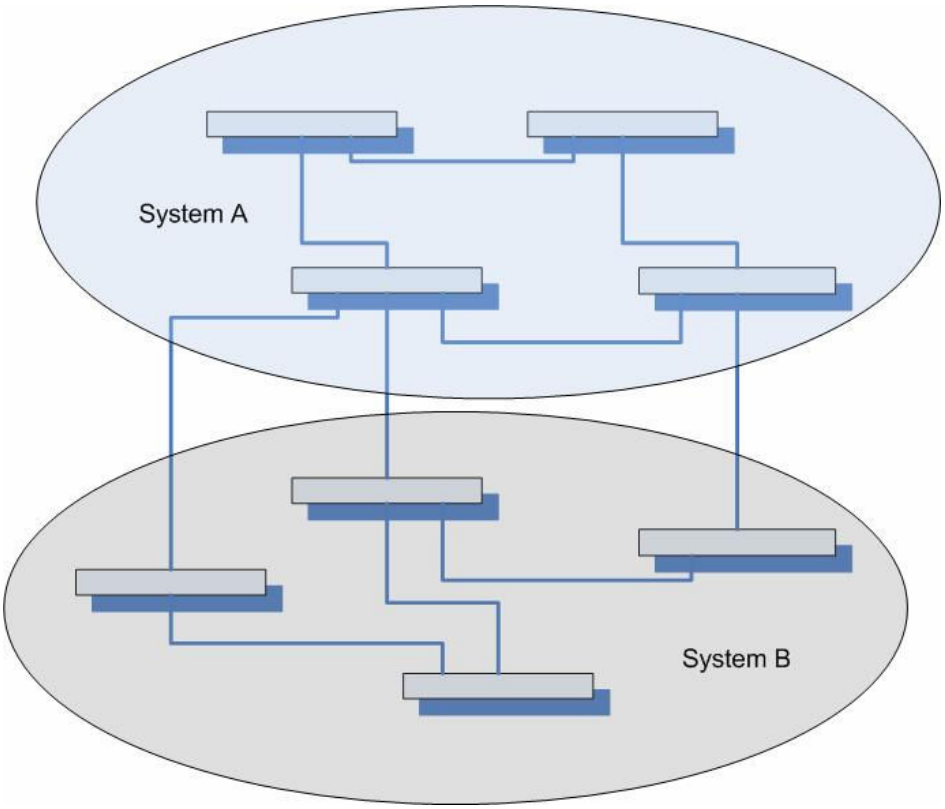

Figure 3.4: Common Tie-line Ownership [10]

The method of Ebrahimian et al. in [19] is decomposed using common boundary bus ownership, yet stands out from other methods because of its use of the "Auxiliary Problem Principle." The central algorithm iterates on an outer loop, which communicates with the area SE's. Each area SE uses virtual measurements at the border, which are functions of the output of the central SE. Essentially, after iteration between central and

area SE's is complete, the solution is optimized and is as accurate as the ISE case. Data transmission is negligible to the amount of time required to run the area SE's over multiple iterations. Bad data detection is handled by both levels and operates effectively. It has been proven that this method converges significantly faster to an optimal solution than the ISE when system size is sufficiently large. However, the area SE algorithms are altered slightly, and multiple area SE runs are required for a single wide area solution resulting in a much larger time commitment than other SSE methods.

3.3 Comparison of Pooling and Processing Time

To understand the reasons for implementing SSE, it is important to quantify the benefits of SSE over ISE, namely in its dramatically decreased data volume and processing requirements. The author in [8] provides the data volume requirements of ISE as compared to SSE. He starts with the case of maximum data transmission, which consists of three major assumptions, namely:

- All active power (P) and reactive power (Q) is measured at the sending and receiving end of each transmission line
- Active and reactive power injection, as well as voltage magnitude are measured at each bus in the system
- The number of branches in the system is roughly equal to twice the number of buses (nbr = 2*nb)

With these assumptions in mind, the size of data transmission is calculated for an ISE containing three individual areas. Designating N as the number of buses, and with the assumption that the number of branches equals 2N, an ISE would require:

Data transmission per area = 2N*4 + N*3 = 11N
Max ISE data transmission = 3*11N (3.1)

Under minimum data transmission, the three assumptions are set as follows:

- P and Q flows monitored at the sending end only

- Voltage magnitude monitored at one bus in the entire network; no power injections are measured
- Ratio of branches to buses in the network equals 1.5

In this case, he finds the data requirements of the ISE to be:

Data transmission per area = 1.5N*2 + 1 = 3N+1
Min ISE data transmission = 9N + 3 (3.2)

In the case of SSE, the data required are the output of the state estimator, along with the measurements along tie-lines. Assuming the data center already has the tie-line information available from its own SCADA system, and recalling that the output of the state estimator is voltage magnitude and angle at all buses, the data to be transmitted can be assumed to be:

Data transmission per area = 2N
Approx. SSE data transmission = 6N

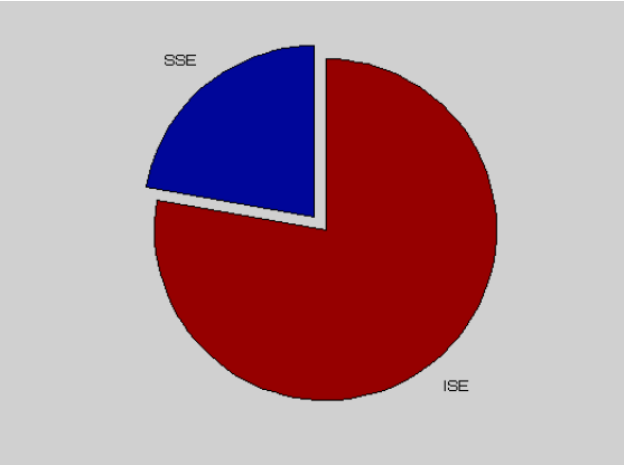

Figure 3.5: SSE vs. ISE Data Volume [8]

As shown in figure 3.5, data transmission of the SSE averages to one third that of the ISE. Notably, however, this is a non-intensive study and the savings factor for data volume does not translate into one for time units. The study simply evaluates the data

volume a central SE controller would contend with for the ISE and SSE cases. In terms of time requirements, the difference between ISE and SSE is not simply a matter of data volume, but one of structural difference as well.

The assumption that network topology remains constant should be revisited when studying the data requirements of SSE. Topology changes must certainly be shared in addition to standard data. Assuming the central SSE operator has an updated model of the system, however, only updates to the previous topology need to be sent for each consecutive SSE execution. Therefore, topology data can be seen as dynamic data volume, and because topology status is a requirement of the ISE and the SSE, it can be concluded that it has a negligible effect on time savings.

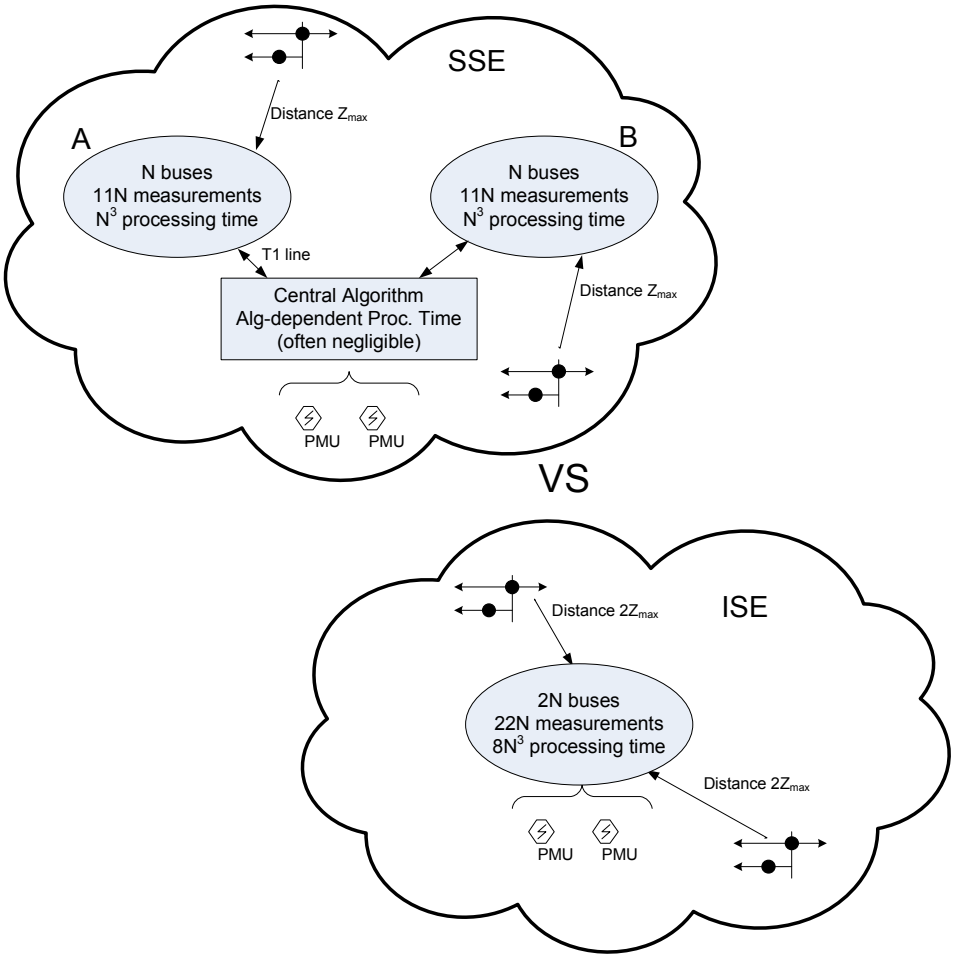

Figure 3.6: SSE vs. ISE Overview

There are two factors besides static data volume to the central controller that affect the total time commitment of the SSE and ISE. Firstly, assuming a configuration as in figure 3.6, individual area SE's poll their own SCADA system for data under the SSE system, while the central estimator pools the entire system under the ISE setup. Therefore, using the maximum data transmission assumption as in equation (3.2), the SSE has a first-level pooling requirement of 11N measurements over a maximum distance Z_{max}. All individual areas have this requirement and therefore area SE's are assumed to be completed simultaneously, regardless of how many areas are in the system. Under the ISE setup, the pooling requirement increases linearly with the number of areas involved. In figure 3.6 with two areas, first level pooling for ISE requires 22N measurements over a $2Z_{max}$ maximum distance. The SSE also requires a second-level pooling requirement in which the central estimator pools the SE outputs, PMU data, and boundary information from each individual area. Because of the small number of data transmitters, investment in high-speed internet-based hubs becomes appropriate. Therefore, the SSE becomes a candidate for information sharing via high-speed internet packet transfer [10], which effectively makes the second-level pooling time requirement negligible in comparison to first-level.

The second major factor affecting time requirement of SSE and ISE is the algorithm processing time. Recall from section 2.3 that the processor requirement of WLS SE increases as the cube of the number of states. Seen in figure 3.6, each SSE area computes its SE independently and simultaneously, requiring N^3 operations regardless of the number of areas present in the system. Furthermore, the central processor requirements of the SSE, while dependent on the number of areas in the system, will be proven to be small in comparison to the area-level computations under methods tested in this thesis. For the ISE, the processor requirement increases with the number of areas present. With two areas, $(2N)^3$ operations are required, with three $(3N)^3$ and so on. Therefore, while the time requirements of the ISE increase exponentially with the addition of areas, those of the SSE method increase linearly and are therefore negligible in comparison.

Chapter 4 - SSE Algorithm Development

To successfully merge the outputs of two neighboring SE's, the SSE method calculates the voltage angle reference of system B with respect to that of system A. Essentially, A's slack node is selected as the global reference, and B's voltage angle reference is assumed to be φ_{diff} degrees behind that of system A. Therefore, adding φ_{diff} to all buses in system B effectively merges that system with A. The estimation of φ_{diff} consequently, is the main task of SSE. This chapter poses four separate algorithms for the calculation of φ_{diff}, along with the method used to compare these methods under the criteria posed in section 1.2.

4.1 Direct Pi-equivalent Method

The pi-equivalent method proposed in [10] is designed to calculate φ_{diff} in a fast, linear manner, with a minimum of data transmission.

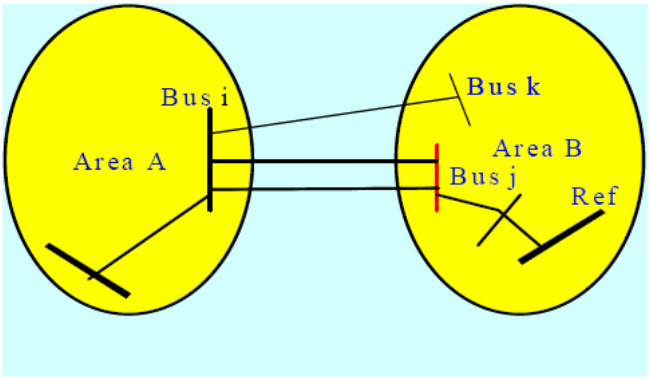

Figure 4.1: Tie-line Representation [8]

In reference to figure 4.1, bus *i* is a boundary bus with voltage angle estimate θ_i on system A's reference [2]. Bus *j* is on the opposite side of a tie-line from *i*, with an angle estimate of δ_j on system B's reference. Using the measured complex power flow from *i* to *j*, the voltage of *j* with respect to system A's reference is calculated as:

$$\overline{V}_b = \overline{V}_a - \overline{Z}_{ab}\left(\frac{\overline{S}_{ab}}{\overline{V}_a}\right) \tag{4.1}$$

where:

Z_{ab} = Impedance of tie line from *i* to *j*

S_{ab} = Power flow along tie line from *i* to *j*

In essence, this method creates an area of overlap by "reaching out" and estimating voltages across tie-lines, resulting in no need for initial overlap in the SE. Once there are two estimates for the angle at bus *j*, the reference angle is simply the difference, $\varphi_{diff} = \theta_j - \delta_j$. With *m* tie lines, there exists the possibility for *2m* calculations for φ_{diff} because of the existence of *from* and *to* power flow measurements on each line:

$$\phi_{calc} = \begin{bmatrix} \theta_1 - \delta_1 \\ \vdots \\ \theta_{2m} - \delta_{2m} \end{bmatrix} \tag{4.2}$$

$$\phi_{diff} = \sum_{i=1}^{2m} (\phi_{calc\,i}) / 2m \tag{4.3}$$

φ_{diff} is added to voltage angles in B, as shown in figure 4.2**,** to reference all voltage angles in B to that of system A [8].

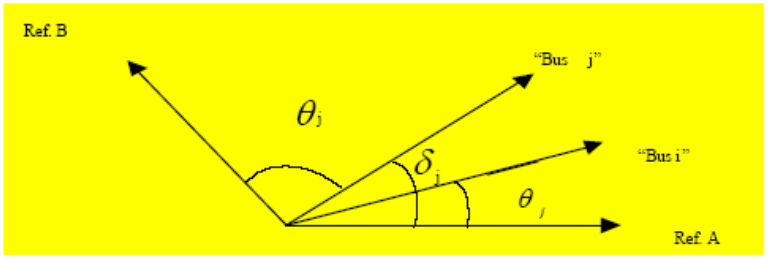

Figure 4.2: Adjustment of Reference Angle [8]

Referencing equation (4.1), the direct pi-equivalent method uses only boundary power flow measurements and boundary voltage estimations to perform its calculation. This data set is common to all three methods, and fulfills constraint 1 in section 1.2. Processor requirement for this method is directly proportional to ½ the number of measurements, or *2m*, twice the number of tie-lines. Because the estimation of φ_{diff} is essentially an unweighted average, and does not take into account varying measurement error, the

method is considered non-optimal. Notably, if the number of estimations *2m* is large, bad data may be detected if an outlier can be pinpointed in the vector (4.2).

PMU data can be utilized in this method by adding terms to the function for φ_{diff} (4.3). Given two PMUs – one in area A and one in area B – an accurate measurement of the true voltage angle difference $\Delta\theta_{ab}$ is available. With the voltage angle estimates from each systems state estimator, φ_{diff} is calculated linearly, by:

$$\phi_{diff} = \Delta\theta_{ab} - \theta_{a\_est} - \theta_{b\_est} \tag{4.4}$$

Assuming *n* PMUs in area A and *p* in area B, (4.4) will provide *n*p* more calculations of φ_{diff} for the averaging equation, (4.3). Therefore, even a minimal presence of PMU data contributes robustness to the φ_{diff} estimation through this method. Additionally, if θ_{a_est} and θ_{b_est} are accurately estimated by area SE's, the estimations added by (4.4) will increase the accuracy of the direct averaging method as well.

Because the direct pi-equivalent method uses an unweighted average, highly biased measurements will cause inaccurate estimation of φ_{diff}. Also, because bad data is difficult to detect without a highly populated φ_{calc} vector (4.2), robustness of this method is poor. Essentially, this method lends itself to speed, simplicity, and low data volume.

4.2 Linear Residual Minimization Method

The linear residual minimization (LRM) method attempts to increase accuracy over the pi-equivalent method without requiring additional data or processor time. Essentially, LRM combines real and imaginary measurement residuals into the complex form in order to create a vector of linear functions of φ_{diff}. The task is to minimize $\|S_{meas} - S_{calc}\|_2^2$ over φ_{diff}, where || || constitutes the 2-based vector normalization [20]. S_{meas} is the vector of tie-line complex power flows, composed of real and reactive power flow measurements:

$$S_{meas} = \begin{bmatrix} P_{ab1} + jQ_{ab1} \\ \vdots \\ P_{ab\,2m} + jQ_{ab\,2m} \end{bmatrix} \tag{4.5}$$

S_{calc} is a vector of calculations of power flow corresponding to each S_{meas}:

$$S_{calc} = \begin{bmatrix} V_{a1}\left(\dfrac{V_{a1}^{\ *} - \left(|V_{b1}|\angle(\theta_b + \phi_{diff})\right)^*}{Z_{ab}^{\ *}} \right) \\ \vdots \end{bmatrix} \tag{4.6}$$

In this sense, each $S_{meas\,i} - S_{calc\,i}$ represents a residual, where $S_{meas\,i}$ is a combination of real and reactive flow measurements, and $S_{calc\,i}$ is a function of the variable φ_{diff}. Therefore, the minimization function of interest is expressed as:

$$R(\phi) = \min_{\phi} \left\| \begin{bmatrix} \vdots \\ S_i^{\ meas} - \dfrac{|V_{ai}|^2}{Z_{ab\,i}^{\ *}} \\ \vdots \end{bmatrix} + (\cos\phi - j\sin\phi) \cdot \begin{bmatrix} \vdots \\ \dfrac{-V_{a\,i} V_{b\,i}^{\ *}}{Z_{ab\,i}^{\ *}} \\ \vdots \end{bmatrix} \right\|_2^2 \tag{4.7}$$

This problem equates to minimizing $\|x - \alpha y\|$, where x and y are complex vectors and $\alpha = \cos(\phi) - j\sin(\phi)$. The function is expanded as follows:

$$\|x - \alpha y\|^2 = (x - \alpha y)^*(x - \alpha y) = \|x\|^2 - \alpha^* y^* x - \alpha x^* y + \|y\|^2 \tag{4.8}$$

Because it is necessary to take the derivative of (4.8) in order to minimize, the constant terms are dropped and the function simplifies to:

$$\begin{aligned} &= -2\,\mathrm{Re}\left[\alpha x^* y\right] = -2\,\mathrm{Re}\left[(\cos\phi - j\sin\phi)(z_r + jz_i)\right] \\ &= -2\left(z_r \cos\phi + z_i \sin\phi\right) \end{aligned} \tag{4.9}$$

where $x^* y = z_r + j \cdot z_i$. Thus, (4.7) can now be minimized by taking the derivative with respect to φ and setting it equal to zero:

$$0 = -2(z_i \cos\phi - z_r \sin\phi) \rightarrow \underline{\underline{\phi = \tan^{-1}\left(\frac{z_i}{z_r}\right)}} \tag{4.10}$$

Because this calculation requires no iteration, φ_{diff} may be calculated with very little overall cost. The main requirement for processing is in the calculations of $x^* y$ (4.9) and the arctangent (4.10) operation. These calculations are on the order of the number of complex flow measurements, *2m*. Theoretically, the φ_{diff} obtained using the LRM method will result in a locally optimal SSE. However, because it minimizes unweighted complex-power residuals, it is not optimized over the objective function *J(x)*. An alternative for increased accuracy is to normalize the power flow residuals by their standard deviations, as follows:

$$R(\phi) = \min_{\phi} \left\| \frac{S_{meas} - S_{calc}}{\sigma} \right\|_2^2 \tag{4.11}$$

Effectively, each power flow residual is now weighted by the measurement's predicted accuracy. Recall (4.5) which states that S_m is a combination of measured real and reactive power flow, with associated standard deviations. The normalized power flow residual can be expanded into its real and imaginary components as follows:

$$\frac{S_{meas} - S_{calc}}{\sigma} = \frac{(P_m + jQ_m) - (P_c + jQ_c)}{\sigma} = \frac{(P_m - P_c)}{\sigma_P} + j\frac{(Q_m - Q_c)}{\sigma_Q}, \sigma_P = \sigma_Q \tag{4.12}$$

From equation (4.12) it is apparent that if σ_P and σ_Q are not equal, then the real and imaginary normalized residuals cannot be combined in the form of equation (4.11) necessary for linear minimization. Herein lays the cause for the sub-optimality of this

method. As a compromise, however, it is prudent to use the square root of the sum of the squares for σ:

$$\sigma = \sqrt{\sigma_P{}^2 + \sigma_Q{}^2} \tag{4.13}$$

The LRM method is capable of incorporating PMU measurements into its minimization function. Recall equation (4.4), which expresses φ_{diff} as a function of PMU measurements and pre-estimated voltage angles. This equation is altered to the form $\|x - \alpha y\|$ in the following manner:

$$1\angle\theta_{meas} - 1\angle\theta_{calc} = 1\angle(\Delta\theta_{ab} - \theta_{a\_est} - \theta_{b\_est}) - (\cos\phi - j\sin\phi)\cdot 1 \tag{4.14}$$

This represents a residual which can be normalized with the standard deviation of $\Delta\theta_{meas}$ as:

$$\frac{1\angle\theta_{meas} - 1\angle\theta_{calc}}{\sqrt{\sigma_{\theta a}{}^2 + \sigma_{\theta b}{}^2}} \tag{4.15}$$

Equation (4.15) can therefore be appended to the vector of normalized residuals in equation (4.11), effectively adding both accuracy and robustness to the LRM method. Bad data may be detected by setting a threshold for *R(φ)* and identified by the highest normalized residual. The LRM is expected to be an improvement over the direct pi-equivalent method in speed and robustness. The inclusion of measurement weighting makes the method slightly less simple, but brings the addition of accuracy from the minimization of weighted residuals. Additionally, the LRM method is not optimal over the SE's minimization function *J(x)* (2.3) because of the simplifying operations performed in (4.5) and (4.13).

4.3 Boundary SE Method

Because the measure of accuracy for the SE is the value of the minimization function, *J(x)*, it is prudent to estimate φ_{diff} such that *J(x)* is locally minimized. The boundary SE method uses the WLS SE technique as outlined in section 2.2 to minimize weighted measurement residuals along the tie lines. The WLS minimization function is formulated as:

$$\min_{\phi} J(\phi) = \sum_{i=1}^{N_m} \frac{\left[z_i^{meas} - f_i(\phi)\right]^2}{\sigma_i^2} \tag{4.16}$$

In the boundary SE method, the only state being estimated is the reference angle difference, φ_{diff}. Measurements such as boundary injections, tie-line flows, and voltage angle differences from PMUs make up the vector of residuals. Recall the update step for the WLS SE:

$$\Delta x^{est} = \left([H]^T[R^{-1}][H]\right)^{-1}[H]^T[R^{-1}](z^{meas} - f(x^{(k)}) = G^{-1}F(x^{(k)}) \tag{4.17}$$

where:

H $\in \Re^{N_m}$ (has dimensions N_m by 1)

R is a diagonal matrix containing σ_i^2's

G $\in \Re$ (has dimension of 1)

Because the estimator has one variable and a small number of measurements, processor requirements are low and it converges quickly. Revisiting the estimations made in section 2.3, the exponential processor requirements nested in the Cholesky decomposition of *G* and the backsolve operation are nonexistent because *G* has dimension of 1. Therefore, processor requirements per iteration are related to $3N_m=12m$. Data volume is also equivalent to the weighted LRM method.

PMU measurements are easily incorporated into the boundary SE method. The measurement vector may be appended as follows for each combination of PMU's in system A and B:

$$z_{pmu} = \begin{bmatrix} \vdots \\ (\Delta\theta_{ab})_i \\ \vdots \end{bmatrix} \tag{4.18}$$

The function vector is appended with:

$$f_{pmu}(\phi) = \begin{bmatrix} \vdots \\ \theta_{a\_est} - (\theta_{b\_est} + \phi) \\ \vdots \end{bmatrix} \tag{4.19}$$

Finally the covariance matrix, *R*, grows diagonally as:

$$R_{pmu} = \begin{bmatrix} \ddots & & \\ & \sqrt{\sigma_{\theta a}{}^2 + \sigma_{\theta b}{}^2} & \\ & & \ddots \end{bmatrix}. \tag{4.20}$$

Since the boundary SE method uses the same minimization criteria as the WLS SE, it offers a locally optimal approximation of φ_{diff} that will therefore minimize the global *J(x)* under the given constraint of no change to area SE's in section 1.2. In addition to being accurate, the boundary SE method is relatively robust because of its ability to handle bad data. Bad data detection and identification are implemented in the manner described in section 2.4.

4.4 Non-linear Residual Minimization Method

The non-linear residual minimization method (NLRM) arises from using only tie-line flow measurements and rewriting equation (4.16) in a vector-norm notation as:

$$J(\phi) = \min_{\phi} \left\| \begin{matrix} \dfrac{P_{mi} - P_{ci}}{\sigma_{P_i}} \\ \dfrac{Q_{mi} - Q_{ci}}{\sigma_{Q_i}} \\ \vdots \end{matrix} \right\|_2^2 \tag{4.21}$$

From the definition of the 2-based vector normalization [20], equation (4.21) and (4.16) are equivalent. To further simplify (4.21), the equations for the power calculations are examined:

$$P_c = \frac{|V_a|^2}{Z_{ab}} \cos(\theta_z) - \frac{|V_a||V_b|}{Z_{ab}} \cos(\underbrace{\theta_z + \delta_{ab}}_{\eta} - \phi) \tag{4.22}$$

$$Q_c = \frac{|V_a|^2}{Z_{ab}} \sin(\theta_z) + \frac{|V_a|^2 B_{ab}}{2} - \frac{|V_a||V_b|}{Z_{ab}} \sin(\underbrace{\theta_z + \delta_{ab}}_{\eta} - \phi) \tag{4.23}$$

The constant terms η are separated from the variable φ_{diff} by using the trigonometry identity transformation in (4.24):

$$\begin{aligned} \cos(\eta - \phi) &= \cos(\eta)\cos(\phi) + \sin(\eta)\sin(\phi) \\ \sin(\eta - \phi) &= \sin(\eta)\cos(\phi) - \cos(\eta)\sin(\phi) \end{aligned} \tag{4.24}$$

Upon the transformation of (4.22) and (4.23), both are in a similar form, and therefore the vector minimization function (4.21) can be written as:

$$J(\phi) = \min_{\phi} \left\| X + Y\underbrace{\cos(\phi)}_{\alpha} + Z\underbrace{\sin(\phi)}_{\beta} \right\|_2^2 \tag{4.25}$$

Notice that this form is similar to that of the LRM method in (4.8), in that *X*, *Y*, and *Z* are now constant vectors, with the variable φ_{diff} removed. The steps for simplifying *J(φ)* are also similar to the LRM method. First *J(φ)* is expanded as follows:

$$\begin{aligned} J(\phi) &= \min_{\phi}(X + \alpha Y + \beta Z)^T (X + \alpha Y + \beta Z) \\ &= \min_{\phi} \alpha \cdot \underbrace{2X^T Y}_{A} + \beta \cdot \underbrace{2X^T Z}_{B} + \alpha\beta \cdot \underbrace{2Z^T Y}_{C} + \alpha^2 \cdot \underbrace{Y^T Y}_{D} + \beta^2 \cdot \underbrace{Z^T Z}_{E} \end{aligned} \tag{4.26}$$

Because of the expansion, *J(φ)* now consists of one non-linear equation of one variable and five constant parameters, and can be written in finalized form by substitution of α and β:

$$J(\phi) = \min_{0 \le \phi \le 2\pi} A\cos(\phi) + B\sin(\phi) + C\cos(\phi)\sin(\phi) + D\cos^2(\phi) + E\sin^2(\phi) \tag{4.27}$$

Equation (4.27) is minimized over the given interval by taking the first derivative with respect to φ, equating to zero, and using Newton's method to solve the non-linear equation. This method excels in computing requirements over the Boundary SE method because vector multiplication is performed before the Newton step.

Of particular note, equation (4.27) has the possibility of local extrema, so therefore a good starting point for φ is critical. In testing with power system data, however, equation (4.27) consisted of only global maximum and minimum. In practice, a good initial guess can be obtained by continuously tracking the result of equation (4.4) using PMU data. When PMU data is not available, the fast linear LRM method may otherwise be employed to locate the starting point. A good initial guess will also have the effect of decreasing the number of Newton iterations needed. Because this method effectively minimizes the same function as the Boundary SE method, bad data detection and elimination are handled in the same manner.

Adding PMU-based equations into the minimization function of (4.21) is difficult unless equation (4.25) is intelligently altered. The key realization is that, because of their

linearity, normalized residuals consisting of PMU measurements have a different form than those built on power flow measurements. Inasmuch, normalized residuals corresponding to PMU measurements have the following form:

$$r_{N\,pmu} = \frac{\phi_{meas} - \phi_{calc}}{\sigma_{pmu}} = q + r\phi$$
$$\text{where,} \quad q = \frac{\Delta\theta_{ab} - (\theta_a - \theta_b)}{\sigma_{ab}} \quad \text{and} \quad r = 1/\sigma_{ab} \tag{4.28}$$

Recall, two PMU's are involved in each $\Delta\theta_{ab}$ measurement, whereas θ_a and θ_b are assumed to be exact quantities taken from the area state estimator. This is a valid assumption if local area state estimators are accurate. The standard deviation used to weight the residual in (4.28) is the square root of the variance of two PMU devices in tandem, or:

$$\sigma = \sqrt{\sigma_A{}^2 + \sigma_B{}^2} \approx \sigma_A \tag{4.29}$$

The PMU equations are placed in vector form, with constant vectors Q, R, and minimized over the variable φ_{diff}, such that they may be appended to (4.25) as:

$$J(\phi) = \min_{\phi}\left[\left\| X + Y\underbrace{\cos(\phi)}_{\alpha} + Z\underbrace{\sin(\phi)}_{\beta}\right\|_2^2 + \left\|Q + R\phi\right\|_2^2\right] \tag{4.30}$$

Expanding the appended equation using the definition of the vector 2-norm yields:

$$\left\|Q + R\phi\right\|_2^2 = \underbrace{2Q^T R}_{F}\phi + \underbrace{R^T R}_{G}\phi^2 \tag{4.31}$$

Therefore, we may once again write *J(φ)* as a single non-linear equation, and equation (4.27) now becomes:

$$J(\phi) = \min_{0 \le \phi \le 2\pi} A\cos(\phi) + B\sin(\phi) + C\cos(\phi)\sin(\phi) + D\cos^2(\phi) + E\sin^2(\phi) + F\phi + G\phi^2 \tag{4.32}$$

As with equation (4.27), equation (4.32) is also solved by equating the derivative to zero and solving with Newton iterations. The only additional computation costs are the calculations of constants F and G through vector multiplication. The results of this method are mathematically equivalent to those of the boundary SE method.

4.5 Procedure for Method Comparison

The IEEE 118-bus system was selected as the power system model for comparing the ISE and SSE methods. A flowchart of the algorithm used for comparison can be viewed in figure 4.3 [8].

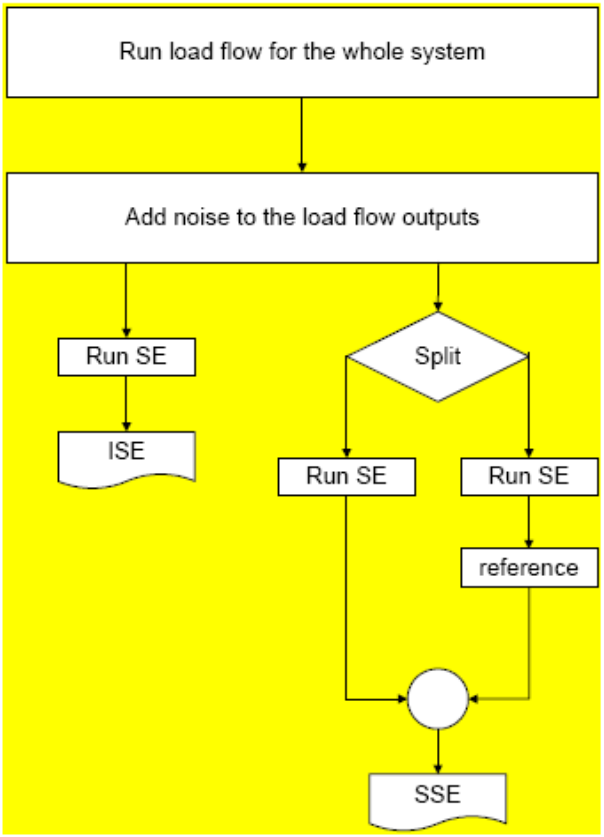

Figure 4.3: Method Comparison Flowchart [8]

Because the state estimation tool used is MATLAB-based, the testing method is also coded in MATLAB. The algorithm runs the ISE and SSE from the same measurement pool, and iterates over several distributions of measurement noise to provide an accurate method comparison.

1. The measurement vector for both ISE and SSE is obtained as follows:

A full-system snapshot is obtained using a loadflow program. PowerWorld was selected for altering system parameters based on its GUI and its relative ease of editing large power systems, yet loadflow simulations were commonly run using PSS/E. The exact power system data and the calculated errors are arranged in the following manner:

$$Z_{exact} = \begin{bmatrix} \mathrm{Re}(S_f) \\ \mathrm{Re}(S_t) \\ \mathrm{Re}(S_{bus}) \\ \theta_v \\ \mathrm{Im}(S_f) \\ \mathrm{Im}(S_t) \\ \mathrm{Im}(S_{bus}) \\ |V| \end{bmatrix}, \; E_Z = \begin{bmatrix} nrand(\sigma_{Pf}) \\ nrand(\sigma_{Pt}) \\ nrand(\sigma_{Pbus}) \\ nrand(\sigma_{\theta v}) \\ ...(imag)... \end{bmatrix} \tag{4.30}$$

Where:

S_f = subvector of "from" flows

S_t = subvector of "to" flows

S_{bus} = subvector of bus power injections

Θ_v = subvector of bus voltage angles from PMUs

$|V|$ = subvector of bus voltage magnitudes

nrand = normal random function in MATLAB with zero mean, standard deviation σ

vv = measurement selection matrix, $vv_{ii}=1$ if z_i^{meas} is to be used

E_z = the vector of normal random noise

The noise is assumed to be zero-mean, normal distribution, with standard deviation proportional to the size of the measurement as calculated in per-unit as:

$$\sigma_i = 0.005 \cdot |Z_i| + 1 \times 10^{-10} \tag{4.31}$$

To create a more realistic error distribution, each error in E_z as shown below is cut off at +/- $3\sigma_i$. From these error calculations, the measurement vector z^{meas} can be created as follows:

$$\begin{gathered} (Z_{exact}) + (E_Z) = (Z_z) \\ \begin{pmatrix} Z_1 \\ \vdots \\ Z_n \end{pmatrix}' \cdot \begin{pmatrix} 0 & 0 & 0 & \\ 0 & 1 & 0 & \dots \\ 0 & 0 & \dots & \\ & \dots & & 1 \end{pmatrix}_{vv} = Z_{meas} \end{gathered} \tag{4.32}$$

To emulate the measurement selection of a true-to-life area SE, flows are measured on both sides of each branch, injections are measured at buses with low measurement redundancy or important load or generation, and PMUs are placed at buses involved in consistently high residuals.

2. System data and measurement data for SSE are obtained as follows:

- Bus territory is designated as two sub-systems in this case (118North, 118South) with no overlap of ownership between.
- Lines that must be symbolically cut to separate the systems are the tie lines.
- The measurement vector and remaining system data are split according to bus territory.

A zoomed-in PowerWorld one-line diagram of one particular split into North and South sub-systems is shown in figure 4.4. The highlighted branches represent the tie-lines between the North and South system.

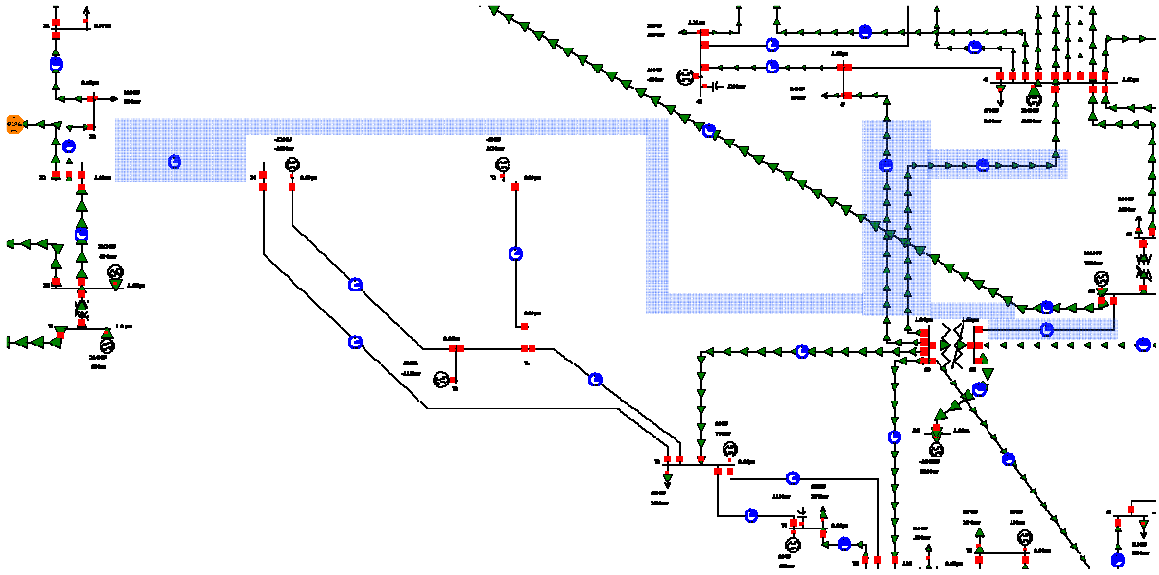

Figure 4.4: One-line Diagram of Tie-line area

Often, because a loss of information is incurred when segmenting the power system in this manner, boundary states are poorly estimated. However, in practice system operators commonly have detailed equivalent models for the systems outside of their area, which improves their estimates at the boundary. To simulate such behavior, each area's SE is configured to estimate two buses into its neighbor, creating a segment of overlap. This extra system information serves the purpose of providing a buffer for the boundary buses. The area inside the blue ellipse in figure 4.5 is the area of simulated overlap for the 118-bus system.

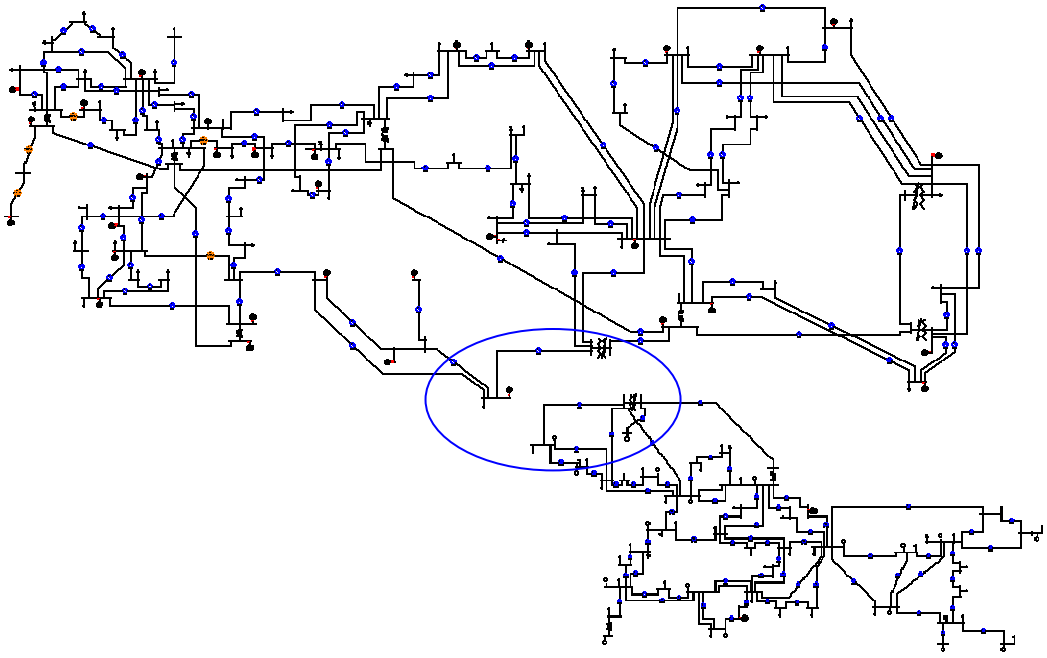

Figure 4.5: IEEE 118 Split N/S With Overlap

3. WLS SE is run for the 118, North, and South systems.

The SE for each system returns the estimated voltage magnitude and angle at all buses, including any added overlap, as well as the vector of normalized measurement residuals for bad data detection.

4. The methods for finding a common reference angle are tested as follows:

Before recombining the SE data from North and South, the added overlap is removed. Recall that its purpose was solely to provide accuracy to the boundary bus estimates. Once the data is pooled, the elected method under scrutiny is used to calculate φ_{diff}. Subsequently, φ_{diff} is added to all voltage angles in the South system, and the SSE is complete. The local *J(x)* spanning the boundary measurements is calculated for the method under test as a measure of each method's local accuracy. A global *J(x)* consisting

of all system measurements is calculated for the SSE using the recombined system, and compared to the ISE's global *J(x)* over the same measurement subset.

Chapter 5 – Results of WASE Methods Comparison

In this chapter, the four SSE methods to calculate φ_{diff} proposed in chapter 4 are judged under the three criteria set forth in section 1.2 as compared to the ISE. All four methods are tested with and without PMU capability, and the LRM method is also tested with and without residual weighting, for a total of 9 method variations, which will be referred to as:

Phi1 = Direct pi-equivalent (4.3) without PMU data
Phi2 = Direct pi-equivalent (4.3) with PMU data (4.4)
Phi3 = Unweighted LRM method (4.7)
Phi4 = Weighted LRM method (4.11) without PMU data
Phi5 = Weighted LRM method (4.11) with PMU data (4.15)
Phi6 = Boundary SE method (4.16) without PMU data
Phi7 = Boundary SE method (4.16) with PMU data (4.19)
Phi8 = NLRM method (4.21) without PMU data
Phi9 = NLRM method (4.21) with PMU data (4.28)

An overview of system parameters and area decomposition is performed in section 5.1. Section 5.2 evaluates each method based on total execution time. The accuracy of each SSE method is determined in 5.3, while their robustness to bad data and abnormal operating conditions are inspected in 5.4.

5.1 System Parameters and Area Decomposition

The procedure outlined in section 4.4 is used with the IEEE 118 bus system to test each SSE method. A system load level of 4580 MW is used, which represents an average mid-morning load based on interpolation from load profiles [21]. The IEEE 118 system contains 118 buses, 187 branches, and 54 bus-connected generators. Real and reactive measurements of power flow are taken at both sides of each branch, giving four flow measurements per branch for a total of 748. Real and reactive injection measurements are placed for local redundancy at 14 buses, providing 28 measurements. Finally, six

PMUs are included as shown in table 5.1, with each measuring voltage magnitude and voltage angle, adding 12 measurements. Therefore with 788 measurements and $2 \cdot 118 - 1 = 235$ states, the ISE case has 553 degrees of freedom (DOF).

Phasor Measurement	Bus No.	Area
1	8	North
2	17	North
3	34	North
4	49	North
5	59	North
6	89	South

Table 5.1: PMU Locations

Areas designated North and South are split according to bus ownership, with North containing 70 buses and South containing 48. In addition, each area SE extends two buses into its neighbor's territory for the sole purpose of providing accuracy to its own boundary bus estimates, extending the estimated area to 78 buses for North and 59 buses for South. This area of overlap, however, is not sent to the central processor when combining North and South to create the SSE. With the additional overlap, the North SE has 363 DOF, while the South system has 253 DOF. As diagramed in table 5.2 and illustrated in figure 4.4, four tie lines separate the North and South systems. Under normal operating conditions, two of these lines are high-flow, and two are low-flow. Five PMUs are available to the North SE, versus only one PMU for south. This simulates a discrepancy commonly found in neighboring systems of differing complexity.

Tie-Line Branch	North Bus	South Bus	$S_{(avg)}$
35	23	24	1.14 - j0.16
74	47	69	0.59 - j0.098
82	49	69	0.49 - j0.12
106	65	68	1.49 - j0.30

Table 5.2: Tie-line Information

5.2 Results of Time Comparison

In this section, the processor time requirement of the ISE is compared to that of the SSE for each combination algorithm. After 5000 iterations, the average processor time required for the ISE, North SE, and South SE are illustrated in table 5.3. Note that because of Matlab's increased efficiency with sparse matrices, the n^3 term for total calculation expense in equation (2.9) is not the dominant term for a system of this small size. However, true power system models are on the order of thousands to tens of thousands of buses, in which case the processor requirements should follow n^3 more closely.

	ISE	North	South
Proc. Time (s)	0.0373	0.0263	0.0182

Table 5.3: ISE vs. Area SE Processor Time

In addition to area SEs, the SSEs processor time requirements are dependent on the central algorithm. Therefore, the simulated processor time for each SSE combination algorithm is illustrated in figure 5.1. In this study, each algorithm was used over 5000 iterations to combine the North and South systems, and the average time elapsed for each algorithm execution was calculated.

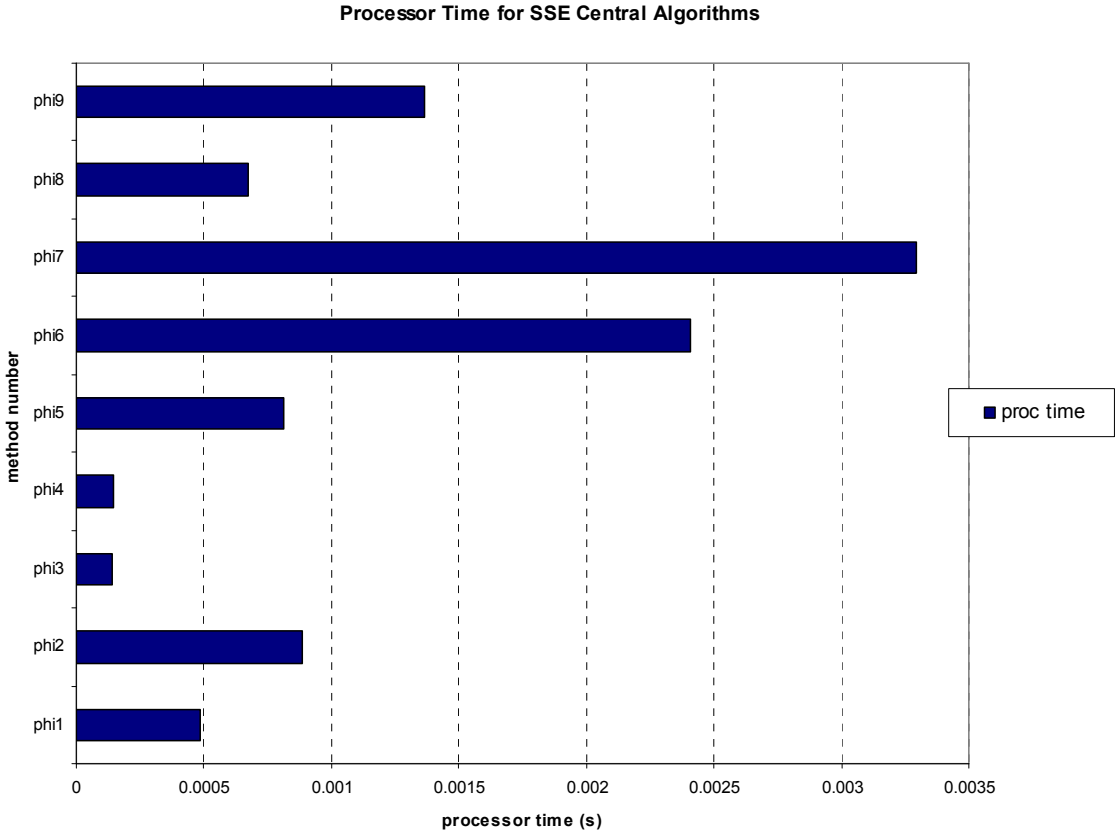

Figure 5.1: Processor Time for SSE Algorithms

Note in figure 5.1 that processor time increases considerably when using PMU data, as illustrated by phi2, phi5, phi7, and phi9. This phenomenon occurs because the ratio of PMU measurements to tie-line measurements is nearly equal, and therefore the addition of the PMU data requires significantly more calculations. Larger systems may or may not have this characteristic. Comparing the two linear methods, there is a nearly negligible time requirement of the LRM method, as compared to the lengthier pi-equivalent method. The vector-based nature of the LRM method versus the for-loop nature of the pi-equivalent method causes the discrepancy because of MATLAB's efficiency with vector calculations. Additionally, when contrasting the two non-linear, locally optimal methods, the NLRM method uses significantly less processor time than that of the Boundary SE.

Recall from section 3.3 that the SSE's total processor requirement equals the sum of its longest area SE time with the computation time of the central algorithm. In this case, the North SE takes the longest, requiring 0.0263s of processor time. Using the unweighted LRM method adds 0.0001s to the calculation time, for a total of 0.0264s. In contrast, the Boundary SE method with PMU data requires an additional 0.0043s for a total processor time requirement of 0.0306s. Contrasting these total times with the ISE's time of 0.0373s, processor time savings for a system of this size are significant, yet not to the factor of 8 as predicted in section 3.3.

5.3 Results of Accuracy Comparison

To judge the accuracy of the proposed WASE methods, the SSE is run using the nine proposed algorithms, while the ISE is run with the same measurement pool. For accuracy comparison, the system is assumed to be under normal operating conditions with all measurements reporting correctly and no topology changes. As noted in section 2.5, the four measures of accuracy for this study are:

- the value of the local WLS SE objective function, J(x), as denoted in equation (2.3), observed over the tie-line flow measurements, i.e. the boundary.

- the value of the global objective function J(x), computed post-SSE processing on the fully combined system, and compared to that of the ISE.
- the accuracy of the voltage magnitude and angle as compared to their true values.
- the accuracy of the estimated reference angle difference, φ_{diff}.

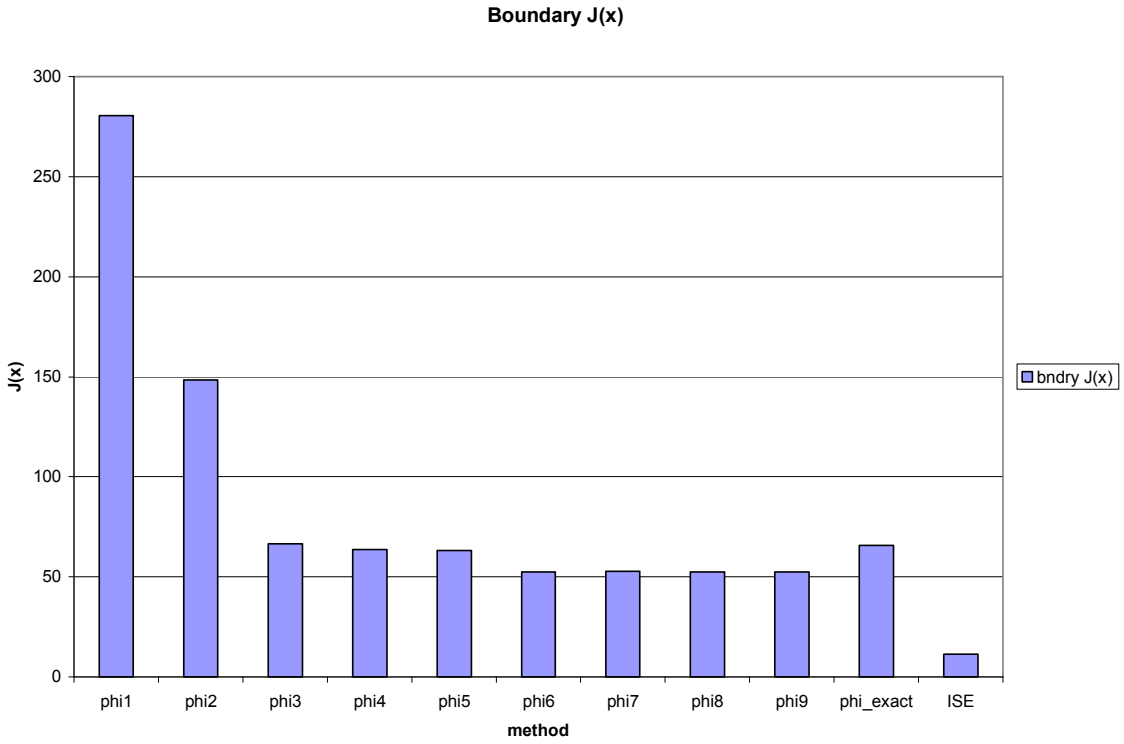

Figure 5.2: J(x) of boundary flows for each method

As previously mentioned, the purpose of the SSE algorithm is to develop a robust estimate of the difference in angle reference between the systems by minimizing boundary residuals. *J(x)* at the boundary is the indicator of how well a particular method minimizes these residuals. The graph of the boundary objective function for the various SE methods in figure 5.2 shows that the simpler methods do a poor job of minimizing the boundary *J(x)*, and therefore may offer poor estimates of φ_{diff}. Additionally, one may expect the global *J(x)* function – that is the sum of the squared normalized residuals over the measurement set of the entire combined system – to correlate in accuracy to the local boundary *J(x)* function. Table 5.4 shows the results of the accuracy tests for each method averaged over 5000 runs of varying noise from the Gaussian distribution simulating standard measurement errors.

	phi1	phi2	phi3	phi4	phi5	phi6
global J(x)	808.28	678.98	594.12	589.96	589.16	580.5
bndry J(x)	280.53	148.43	66.48	63.61	63.2	52.43
avg Vmag error, pu	5.82E-05	5.84E-05	5.85E-05	5.81E-05	5.79E-05	5.81E-05
max Vmag error	2.127E-04	2.143E-04	2.134E-04	2.130E-04	2.128E-04	2.128E-04
location	24	24	24	24	24	24
avg Vang error, deg	0.0244	0.0169	0.0095	0.0091	0.0088	0.0095
max Vang error	0.0669	0.0493	0.0344	0.0334	0.0331	0.0343
location	24	24	10	10	10	10
avg (φdiff - φexact)	0.048	0.0295	0.0101	0.0088	0.0081	0.0094
	phi7	phi8	phi9	phi_exact	ISE	
global J(x)	580.53	579.97	579.95	593.57	539.74	
bndry J(x)	52.82	52.46	52.46	65.74	11.43	
avg Vmag error, pu	5.82E-05	5.82E-05	5.84E-05	5.85E-05	7.00E-05	
max Vmag error	2.134E-04	2.116E-04	2.13E-04	2.129E-04	2.233E-04	
location	24	24	24	24	112	
avg Vang error, deg	0.0092	0.0096	0.0094	0.0073	0.0087	
max Vang error	0.0337	0.0346	0.0341	0.0322	0.0323	
location	10	10	10	10	10	
avg (φdiff - φexact)	0.0088	0.01	0.0094	0	N/A	

Table 5.4: Results of Accuracy Test for SSE Methods

The value of the global objective function, *J(x)*, gives insight into the overall accuracy of each method. By this measure, the direct pi-equivalent method offers a poor estimation of φ_{diff}, and correspondingly, a poor SSE. The poor φ_{diff} estimate is directly seen by examining the average error of the estimated φ_{diff}. Also, with this method, abnormally large normalized residuals lie on the boundary, which is a direct result of the poor φ_{diff}. In contrast, the LRM method provides a significant increase in overall and local accuracy. The addition of measurement accuracy weighting and PMU data provide incremental accuracy to this method, as well. The two locally optimal methods – those being the boundary SE and the NLRM - give the best minimization of *J(x)* because they locally minimize *J(x)* at the boundary. However, even with local minimization, the normalized residuals on boundary tie-lines remain higher compared to the ISE case. Notably, under these normal operating conditions PMU data does not improve nor hinder the accuracy of these methods, because the additional calculations do not correspond to residuals along the tie-lines, and therefore employing them has little effect to the *J(x)* at the boundary.

5.4 Results of Robustness Testing

To be considered robust, the WASE method in question should be able to detect the presence of bad data and eliminate it. To test the SSE algorithms for bad data detection, an error of 0.5pu is placed on the reactive flow from bus 65 to bus 68, changing the measured flow from 1.4937-i*0.3042 to 1.4937+i*0.1958. First, each area SE should check for the presence of bad data. As outlined in section 2.4, the method for detecting the presence of bad data for the WLS SE is to set a threshold on *J(x)*. With a 95% confidence level, the χ^2 thresholds for the ISE, North, and South systems are shown in table 5.5. They are obtained from tables in [22] on the assumption that the χ^2 distribution is approximately normal at DOF greater than 30, with a mean of the DOF, and a variance of twice the DOF [22].

	ISE	North	South
N_m	788	518	370
N_s	235	155	117
DOF	553	363	253
Threshold	608	407	290

Table 5.5: Threshold Values for J(x)

Applying the threshold test to each SE yields a *J(x)* value of 53872, 390, and 282 for the ISE, North, and South SEs respectively. Therefore, the ISE detects the presence of bad data, while the North and South SEs do not. Additionally, when the largest normalized residual test is applied to the ISE, a normalized residual value of 164 is located on the reactive flow from bus 65 to bus 68, which is the bad data in question. Therefore the ISE succeeds in identifying the bad data.

Because the bad data is located on the boundary, the area SEs rely on the central combination algorithm to detect its presence. With the direct pi-equivalent method, the bad data detection procedure is to search the individual φ_{diff} calculations for outliers. However, with the bad data in question being small in magnitude, no outlier exists under phi1 or phi2, as demonstrated in table 5.6.

Central Algs	phi1	phi2
phi_est for Sf 65-68	-22.49	-22.49
mean phi_est	-22.55	-22.52
detect?	no	no

Table 5.6: Robustness Test for Pi-equivalent

The LRM methods also have difficulty detecting the presence of bad data, partially due to the fact that real and reactive measurements are combined into their complex values. As shown in table 5.7, the total value of the minimization function $R(\varphi)$ does not necessarily dictate the presence of bad data for this case. However, the residuals on the 'from' and 'to' side of the 65-68 tie line are significantly high, and therefore the presence of bad data may be inferred. However, the method fails in identifying which side of the tie-line produces the bad data.

Central Algs	phi3	phi4	phi5
calc phi_est	-22.481	-22.487	-22.484
residual for Sf 65-68	0.020 + 0.180i	1.739 + 23.79i	2.168 + 23.76i
R(phi)	0.145	3.43E+03	3.44E+03
R(phi) with good data	0.215	4.62E+03	4.62E+03

Table 5.7: Robustness Test for LRM

As illustrated by table 5.8, the boundary SE method correctly detects and identifies the bad data placed on the tie-line by testing the local threshold on $J(x)$, and applying the largest normalized residual test. Therefore, it is robust to the presence of bad data along the boundary.

Central Algs	phi6	phi7
J(x)	1.02E+05	1.02E+05
DOF	16	21
threshold	26.3	32.7
detect?	yes	yes
Max rN	9.90E+04	9.94E+04
location	Qf 65-68	Qf 65-68
identify?	yes	Yes

Table 5.8: Robustness Test for Boundary SE

From table 5.9, the NLRM method is shown to be equally robust under the presence of bad data. This is intuitive, because both methods essentially minimize the same function. Therefore, the NLRM method also fulfils this section of the robustness criterion.

Central Algs	phi8	phi9
J(x)	1.06E+05	1.07E+05
DOF	16	21
threshold	26.3	32.7
detect?	yes	yes
Max rN	9.85E+04	9.98E+04
location	Qf 65-68	Qf 65-68
identify?	yes	yes

Table 5.9: Robustness Test for NLRM

For purposes of reliability, the WASE methods should also provide accurate results during abnormal conditions, such as the loss of a tie line. Robustness to abnormal conditions is tested by removing the line between bus 65 and bus 68 from service, and testing the algorithms for proper operation under the loss of data. Table 5.9 demonstrates the change in flow across the remaining tie lines. Branch 35 absorbs most of the additional North-South power flow.

Tie-Line Branch	North Bus	South Bus	$S_{(avg)}$
35	23	24	1.58-j0.26
74	47	69	0.041+j0.014
82	49	69	0.073-j0.096
106	65	68	----------

Table 5.10: Tie-line Load with Branch 106 Out

Under these conditions, the algorithms are stressed by a loss of data as well as an abnormally high flow on the remaining lines. As shown in table 5.11 by the average *J(x)* after 500 iterations, only the non-linear, locally optimal methods are able to overcome these conditions, while the fast, linear, non-optimal methods fail under this criterion. Because the pi-equivalent and LRM methods use non-normalized calculations, the one remaining high-flow line dominates their estimation of φ_{diff} to the point of significant accuracy degradation. Additionally, the presence of PMUs offers robustness to the methods by providing estimates of φ_{diff} that are unaffected by the loss of boundary data.

This observation is illustrated by the improvement in accuracy of phi2, phi5, phi7, and phi9 over their counterparts that do not utilize PMU data.

	phi1	phi2	phi3	phi4	phi5
mean(jx)	689	678.9	961.2	2310	2227
phidiff - phi_exact	0.0126	0.0101	0.0231	0.0661	0.0638
	phi6	**phi7**	**ph8**	**phi9**	**ISE**
mean(jx)	597.4	595.1	595.9	590.2	535.1
phidiff - phi_exact	0.0095	0.0098	0.0101	0.0092	N/A

Table 5.11: Algorithm Accuracy with Loss of Line

Chapter 6 - Conclusions and Future Work

6.1 Objectives and Contributions

This thesis addresses a main concern for the wide area monitoring and control of power systems, namely the creation of a WASE as a primary tool for such functions. The argument has been posed that current monitoring systems are not sufficiently wide scale, and therefore the burden is on current system operators for reliability coordination. Inasmuch, the primary contribution of the thesis work is the testing of realistically feasible methods for WASE. Upon examination of the literature, a hierarchical structure for WASE is found to have benefits in terms of speed and processor requirements. Among the studied methods, two are chosen and two new methods are developed by the author (LRM and NLRM) aimed at satisfying the constraints placed in section 1.2. Essentially, the goal of these constraints is to ensure that the method in question operates without altering the existing SE or requiring sensitive data. Additionally, each of the methods is altered to include the capability of employing PMU data. The methods are tested based on speed, accuracy, and robustness, as compared to the baseline ISE case. Following is a summary of the findings from researching and testing the proposed methods:

- The SSE methods require significantly less data to be passed from operators to the central coordinator than an ISE method, decreasing pooling time and increasing data security.

- On a system such as the IEEE 118, processor time savings for SSE versus ISE are small yet significant. It has been mathematically shown, however, that on large systems, time savings are proportional to the cube of the system size.

- The NLRM method offers a negligible central processing time, locally optimal accuracy, and acceptable robustness. It is the only tested method to satisfy all three criteria. The pi-equivalent method succeeds in simplicity, has moderately low processing requirements, yet is the least accurate of the tested methods and fails robustness testing. The LRM method succeeds in improving accuracy and

processing speed over the pi-equivalent method yet fails under loss of data or bad data situations. The boundary SE method is highly accurate and robust, but its processing time grows exponentially compared to the other two methods.

- While the inclusion of PMU data does little to improve the accuracy of locally optimal methods under normal operating conditions, it offers considerable robustness under loss of tie line data.

Quintessentially, because of the power system's inherent coupling, any attempt at traditional SE on the scale of local operators will result in a loss of external system information, and therefore a loss of accuracy. The buses of a local SE that are most affected by this loss of information are those that are most greatly coupled to the external systems – i.e. buses at the boundary. This is why, in simulation, the difference between the global *J(x)'s* of the SSE and ISE is nearly equal to the difference between their boundary *J(x)'s*. For these reasons, much work into modeling external system equivalents has been done to alleviate boundary errors, to the point where system operators are reasonably confident in their SE solutions. If boundary estimates are indeed accurate, then under normal operating conditions an SSE using a locally optimal method such as NLRM may be nearly as accurate as if an ISE were run. However, the need for wide-area monitoring is rooted in reliability, which requires an SE robust to abnormal conditions. Under such circumstances, external equivalent models to a local SE can fail when a wide-area SE would not. This thesis has shown that the NLRM method possesses the speed, accuracy, and robustness to combine neighboring systems' SE outputs into an SSE suitable for wide-area monitoring.

6.2 Further Study

Several topics of interest arise from the completion of this study. Areas that would help progress toward a better understanding of the feasibility and implementation of WASE are as follows:

- Further study into variations of the LRM method to improve bad data detection and operation under abnormal operating conditions would be beneficial because of the LRM's inherently low processor load.

- Study of SSE time skew related to non-synchronized area SEs is important for establishing a standard coordination operating procedure.

- The ability to coordinate topology changes into the shared data should be investigated to ensure that the added data load is insubstantial.

- The study should be applied to larger, more realistic systems, closely studying the processing requirements and the robustness for the proposed methods under larger sets of data.

7 - References

[1] Merrill, H.M. “Regional transmission organizations: FERC Order 2000” IEEE Power Engineering Review, Vol. 20 Issue: 7, July 2000 pp. 3 –5.

[2] McCartney, Bobbie J. “Proposed Mediation Model for a Southeastern Regional Transmission Organization” Submitted by the SeTrans sponsors, Docket No. RT01-100-000, FERC: August 2001 pp.30-35.

[3] U.S.-Canada Power System Outage Task Force “Final Report on the August 14, 2003 Blackout in the United States and Canada: Causes and Recommendations” April 2004 [online] Available: https://reports.energy.gov/.

[4] Louie, H., Strunz, K. “Hierarchical Multiobjective Optimization for Independent System Operators (ISOs) in Electricity Markets” IEEE Transactions on Power Systems, V. 21, No. 4, November 2006.

[5] G. N. Korres, G. C. Contaxis, “Application of a reduced model to a distributed State Estimator” Power Engineering Society Winter Meeting, 2000. IEEE Volume 2, 23-27 Jan. 2000 Page(s):999 - 1004 vol.2. Dec. 2000.

[6] K.A. Clements, O.J. Denison, and R.J. Ringlee, “A Multi-area Approach to State Estimation in Power System Networks”, Proc. IEEE/PES Summer Meeting, pp. 465-473, Jan. 1973.

[7] T. Van Cutsem, J.L. Horward, and M. Ribbens-Pavella, “A Two-level Static State Estimator for Electric Power Systems”, IEEE Transactions on PAS, vol. PAS-100, pp. 3722-3732, Aug. 1981.

[8] Abdel-Rahman Khatib.. “Internet-based Wide Area Measurement Applications in Deregulated Power Systems”, Dissertation submitted to the Faculty of the Virginia

Polytechnic and State University, pp.31-52. July 2002.

[9] Zhao, Liang. “Multi-area Network Analysis” Dissertation submitted to Texas A&M University, pp.6-34, Dec. 2004.

[10] Abdel-Rahman Khatib. “Internet Based Wide Area Information Sharing and its Roles in Power System State Estimation”, Power Engineering Society Winter Meeting, 2001 IEEE, Vol. 2, 2001, pp. 470 –475. Dec. 2001.

[11] R. Zivanovic, C. Cairns. “Implementation of PMU Technology in State Estimation: An Overview”, IEEE Africon 4th, Volume 2, 24-27 Page(s):1006 – 1011, Sept. 1996.

[12] Phadke, A.G. “Synchronized phasor measurements in power systems”, Computer Applications in Power, IEEE Volume 6, Issue 2, pp.10-15, April 1993.

[13] Bertsch, J. et al. “Experiences with and perspectives of the system for wide area monitoring of power systems” Quality and Security of Electric Power Delivery Systems, CIGRE/IEEE PES International Symposium, pp. 5-9, Oct. 2003

[14] Allen J. Wood, Bruce Wollenberg. “Power Generation, Operation, and Control” a Wiley-Interscience Publication, Chapter 12, pp.455-490, 1996.

[15] Ali Abur, Antonio Gomez Exposito. “Power System State Estimation Theory and Implementation” Marcel Dekker, Inc., Ch. 1-2, pp.1-36, 2004.

[16] Iraj Dabbaghchi, Louis VanSlyck. “Inter-Utility Data Exchange for State Estimation” Power Systems, IEEE Transactions, Volume 3, Issue 3, pp.1254-1262, Aug. 1988.

[17] K. E. Martin. "IEEE Standard for Synchrophasors for Power Systems" IEEE Transactions on Power Delivery, Vol. 13, No. 1, January 1998.

[18] Xu Dongjie et al. "Comparison of Several PMU Placement Algorithms for State Estimation" Developments in Power System Protection, 8th IEE International Conference on. Vol.1, 5-8, pp. 32-35, April 2004.

[19] Reza Ebrahimian, Ross Baldick. "State Estimation Distributed Processing" IEEE Transactions on Power Systems, Vol. 15, No. 4, November 2000.

[20] David Watkins. "Fundamentals of Matrix Computations – Second Edition" a Wiley-Interscience Publication, Chapter 2, pp. 111-125, 2002.

[21] I. Fuyong. "IEEE 118 hourly load data", Obtained freely from Electrical and Computer Engineering Department, Illinois Institute of Technology, motor.ece.iit.edu/Data/, 2006.

[22] J.S. Milton, J.C. Arnold. "Introduction to Probability and Statistics: Principles and Applications for Engineering and the Computing Sciences – Third Edition" McGraw Hill Series in Probability and Statistics, Chapter 4, pp. 100-120, 1995.

[23] Federal Energy Regulatory Commision "RTO Regional Map" September 2006, Available: http://www.ferc.gov/industries/electric/indus-act/rto.asp

8 – Vita

Robert Jeffers was born in Richmond, Virginia of the United States on October 11, 1982. He received his Bachelors degree from Virginia Tech in December of 2004, where he continued his Masters studies in power systems engineering. He has served as a research assistant to professors in the Center for Power Electronic Systems, the Oak Ridge National Lab, as well as the power systems branch of the Electrical and Computer Engineering department at Virginia Tech. In addition to his thesis studies, Robert has studied the viability and integration of renewable energy technologies on both national and community-based levels. He has deep and profound interest in researching technologies that progress towards a sustainable energy system, such as hybrid-electric vehicles, distributed generation and micro-grids, efficient energy storage, and renewable power generation.